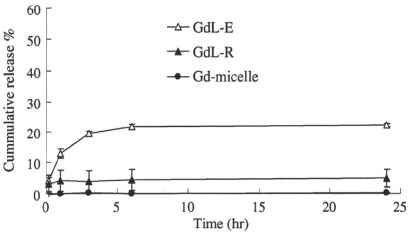

Fig. 2. Release profiles of Gd from Gd-micelle or Gd-DTPA from Gd-liposomes prepared by ethanol injection method (GdL-E) and reverse phase evaporation method (GdL-R) in PBS (pH 7.4) at 37°C. Data represent mean±S.D. (n=3).

Pharmacokinetics of the Gd-micelle and Gd-liposome

As shown in Fig. 3, at 10 min after the intravenous injection, 33.3% of the injected dose was found in blood for the Gd-micelle, and 40.0% and 50.3% for the Gd-liposome of GdL-E and GdL-R, respectively. At a dose of 33 μmol Gd/kg, the $T_{1/2}$ of the Gd-micelle was 10.2±3.9 h. Besides, the $T_{1/2}$ of GdL-E at a dose of 6.75 μmol Gd/kg and GdL-R at a dose of 2.65 μmol Gd/kg were 5.9±0.5 h and 6.0±1.0 h, respectively. In a previous study, we showed that Gd-DTPA was very rapidly cleared from the bloodstream with a minute's order half-life (19). Therefore, the detected Gd in blood is considered to be Gd-DTPA encapsulated in the liposome in a quantitative manner for measurements 6 h post intravenous injection. On the other hand, the main purpose of this study is the ABC phenomenon of a polymeric micelle MRI contrast agent, and PEGylated liposome is used as a positive control for the ABC phenomenon. Therefore, detection of liposome with Gd measurements is appropriate for the present purpose.

Effect of the First Dose on the Distribution of the Gd-micelle

The effects of the first dose on the distribution of the Gd-micelle injected a second time were evaluated. When the second dose of Gd-micelle was fixed at 33 μmol/kg, there was no significant difference of percent injected doses in plasma, kidney, and spleen between various first doses of the Gd-micelle from 0 to 100 μmol/kg (Fig. 4A). A dose of 100 μmol Gd/kg is the clinical dose of Gd-DTPA (17). Interestingly, the distribution of Gd-micelles in plasma, kidney, spleen and liver with the first injection of the empty liposome was similar to that with the first injection of saline. For the liver, the percent injected dose after a first dose of 33 μmol/kg and 100 μmol/kg was significantly higher than in the control saline group, possibly due to the incomplete elimination of the first dose of the Gd-micelle in liver at day 7 because of high doses of polymeric micelles (67.3 mg ~ 203.9 mg polymer/kg). The dose of 2 μmol Gd/kg of the Gd-micelle was the minimum at which Gd was detectable by means of ICP 6 h after injection. As shown in Fig. 4B, when the second dose of the Gd-micelle was decreased to 5 μmol/kg and 2 μmol/kg, the distribution was similar to that of 33 μmol/kg (Fig. 4A). Hence, the results showed that the tissue distribution of the Gd-micelle at the second dose of 33, 5, or 2 μmol/kg was not affected significantly except in liver by pre-administration of the Gd-micelle or the empty liposome. Although Gd in the first dose may interfere with the Gd accumulation in liver following the second dose injection, Gd-micelle as the first dose for micelle-forming properties are

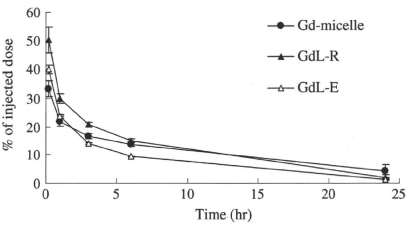

Fig. 3. Plasma elimination profiles of Gd following a single intravenous injection of Gd-micelle at a dose of 33 μmol Gd/kg and Gd-liposome including Gd-liposome prepared by ethanol injection method (GdL-E) at a dose of 6.75 μmol Gd/kg and Gd-liposome prepared by reverse phase evaporation method (GdL-R) at a dose of 2.65 μmol Gd/kg. Data represent mean±S.D. (n=3–4).

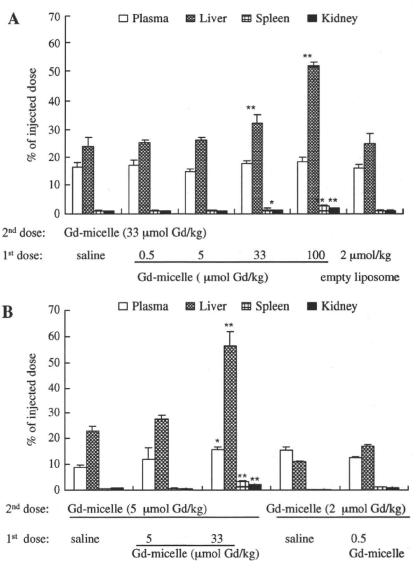

Fig. 4. Effect of the first dose on the tissue distribution of Gd-micelle. The second dose of Gd-micelle with 33 μmol/kg (**A**) or 5 μmol/kg or 2 μmol/kg (**B**) was intravenously injected at day 7 after the first injection of 0.5, 5, 33, 100 μmol/kg of Gd-micelle or the empty liposome at a dose of 2 μmol lipid/kg. Tissues including blood, liver, spleen, and kidney were taken out 6 h after the second injection of Gd-micelle. Data represent mean±S.D. (n=3, 6). P values apply to differences between the saline group and Gd-micelle or liposome treated group. *p<0.05, **p<0.01.

Gd-content-dependent, and Gd-free polymeric micelle is different from the Gd-containing micelle in size and micelle forming characteristics.

Effect of Time Interval Between the Two Injections on the Distribution of the Gd-micelle

Since it was reported that the ABC effect was maximized when the interval between the two injections of liposome was 10 days in mice (7,12), we changed the time interval for the injection of Gd-micelle at a dose of 33 μmol/kg from 3 days to 10 days. No significant difference in plasma Gd levels (15 ~ 18% dose) was observed between the control group and the groups with different time intervals 6 h after the second injection (Fig. 5). The control group was given the Gd-micelle at 33 μmol/kg after a first injection of saline. The Gd% of injected dose in the liver was much higher at day 3 after the second injection than that on other days, probably due to the incomplete elimination of the first dose of the Gd-micelle.

Effect of the First Dose on the Distribution of the Gd-liposome

Since a lower dose of lipid in the first injection results in a more significant ABC, the effects of dose were investigated. The first dose of the Gd-micelle (5 μmol Gd/kg), empty GdL-E (2 μmol lipids/kg), or GdL-E (2 μmol lipids/kg corresponding to 0.45 μmol Gd/kg) was given with a second dose of GdL-E at 10 μmol lipids/kg corresponding to 2.26 μmol Gd/kg. As shown in Fig. 6, the first injection of the Gd-micelle resulted in a similar percentage of the injected dose of the Gd-liposome in plasma, liver, spleen, and kidney in comparison with the saline group. On the other hand, after the second injection of GdL-E, the Gd concentrations in plasma and kidney were too low to be detected, with the first injection of the empty GdL-E and the GdL-E. At that time, the %dose in the liver significantly increased, but that in spleen significantly decreased as compared to saline ($p<0.05$).

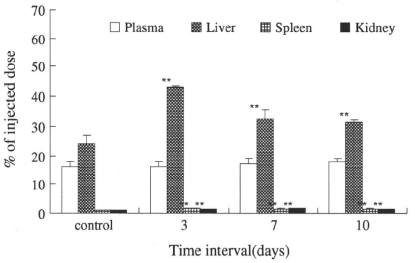

Fig. 5. Effect of the time intervals on the tissue distribution of Gd-micelle. The second dose of Gd-micelle at 33 μmol/kg was intravenously injected at day 3, day 7, or day 10 after the first injection of the same micelle at 33 μmol/kg. The control group was referred to the second dose of Gd-micelle at a dose of 33 μmol/kg with the first injection of saline. Tissues including blood, liver, spleen, and kidney were taken out at 6 h after the second injection of Gd-micelle. Data represent mean±S.D. ($n=3$). *P* values apply to differences between the control group and treated group. $*p<0.05$, $**p<0.01$.

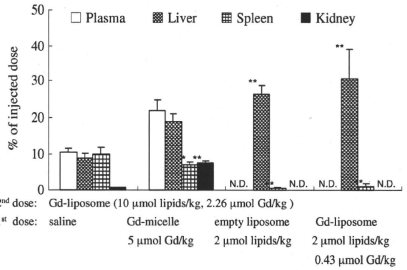

Fig. 6. Effect of the first dose on the tissue distribution of Gd-liposome (GdL-E). The second dose of GdL-E with 10 μmol lipids/kg and 2.26 μmol Gd/kg was intravenously injected at day 7 after the first injection of Gd-micelle (5 μmol Gd/kg), empty GdL-E (2 μmol lipids/kg), and GdL-E (2 μmol lipids/kg and 0.43 μmol Gd/kg). Tissues of blood, liver, spleen, and kidney were removed 6 h after the second injection of GdL-E liposome. Data represent mean±S.D. ($n=3$). *P* values apply to differences between the saline group and Gd-micelle or liposome treated group. $*p<0.05$, $**p<0.01$. N.D. The Gd concentration was too low to be detected by ICP.

Therefore, the data herein show that the accelerated clearance of Gd-liposome at 10 μmol lipids/kg corresponding to 2.26 μmol Gd/kg was induced by both the Gd-liposome and empty liposome, but not by the Gd-micelle. This finding indicates that Gd ions at the first dose of 0.45 μmol/kg did not affect the induction of ABC caused by liposomes.

Effect of PEG on the Distribution of Gd-liposomes

Next, the effect of injecting a PEG homopolymer and PEG_{2000}-DSPE on the distribution of Gd-liposomes was examined. Since the encapsulation efficiency of Gd was low with the ethanol injection method, we prepared another Gd-liposome by the reverse phase evaporation method (GdL-R). The tissue distribution of GdL-R at 6 h after injection at a dose of 5 μmol lipids/kg was not significantly influenced by the pre-administration of 50 mg/kg PEG $_{500,000}$, 0.2 mg/kg PEG $_{500,000}$, or 0.3 mg/kg PEG_{2000}-DSPE 7 days before (Fig. 7). The dose of 0.2 mg/kg PEG $_{500,000}$ and 0.3 mg/kg PEG_{2000}-DSPE with the concentration of 0.04 mg/ml is similar to that of the 5 mol% PEGylated liposome (0.3 mg/kg PEG_{2000}-DSPE), which could produce the ABC phenomenon (Fig. 6). Hence, the first injection of $PEG_{500,000}$ saline or PEG_{2000}-DSPE saline failed to cause the ABC phenomenon after the second administration of Gd-liposome. Hence, only injections of PEG macromolecules did not induce the ABC effect.

DISCUSSION

In the present study, the influence of dose on the tissue distribution of Gd-micelles after repeated administrations was investigated. Many studies have found that a lower dose of lipid in liposomes or nanoparticles results in a greater ABC effect (6–8,12), and the magnitude of the ABC phenomenon reached a maximum when the time interval between two

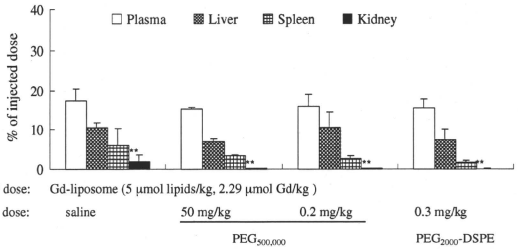

Fig. 7. Effect of $PEG_{500,000}$ and PEG_{2000}-DSPE on the tissue distribution of Gd-liposome (GdL-R). The second dose of Gd-liposome with 5 μmol lipids/kg and 2.29 μmol Gd/kg was intravenously injected at day 7 after the first injection of $PEG_{500,000}$ saline at a dose of 50 mg/kg or 0.2 mg/kg, and PEG_{2000}-DSPE saline at 0.3 mg/kg. The control group of GdL-R was injected at a dose of 10 μmol lipids/kg with the first injection of saline. Tissues of blood, liver, spleen, and kidney were removed at 6 h after the second injection of GdL-R. Data represent mean±S.D. (n=3–5). P values apply to differences between the saline group and $PEG_{500,000}$ or PEG_{2000}-DSPE treated group. $*p<0.05$, $**p<0.01$.

injections was 5–7 days in rats (5) and 10 days in mice (7,12). Hence, we investigated the distribution of the Gd-micelle at various doses and an interval of 3, 7, or 10 days between injections. We found that repeated injections of the Gd-micelle, even with the second dose reduced to 2 μmol Gd/kg (corresponding to 4 mg polymer/kg) and at different time intervals at a dose of 33 μmol Gd/kg (corresponding to 67.3 mg polymer/kg), did not result in an accelerated clearance. ABC of the second injection of the Gd-liposome was induced by the first injection of both the Gd-liposome and the empty PEGylated liposome, but not by the first injection of the Gd-micelle (Fig. 6), Gd-DTPA encapsulated in liposomes would not affect the ABC phenomenon. Therefore, our observation that the ABC phenomenon did not occur with the Gd-micelle is important as it means that injections of the Gd-micelle will not change the biodistribution of a second administration of diagnostic or therapeutic agents.

For Gd-micelle, Gd was chelated to the micelle and thus existed in the form of micelle as shown in Fig. 1, which was consistent with the release results in Fig. 2 that Gd did not leak from the Gd-micelle in PBS (pH 7.4). Gd concentration in plasma, therefore, will reflect the pharmacokinetic behavior of the Gd-micelle. For Gd-liposomes, although the Gd concentration in plasma contained both the leaked Gd-DTPA from the Gd-liposome and the encapsulated Gd-DTPA in the Gd-liposome, the leaked-free Gd-DTPA is reported to be very rapidly cleared from the bloodstream with a minute's order half-life (19), and thus the detected Gd in blood is considered to be only the Gd-DTPA encapsulated in the liposome 6 h after intravenous injection in this study. Compared to GdL-R, the leakage of Gd-DTPA from GdL-E was faster, resulting in the lower Gd concentration (the encapsulated Gd) of GdL-E in blood in Fig. 3. Most importantly, the purpose of this study is to investigate if the distribution for the second dose of the Gd-liposomes or Gd-micelle was affected after pre-administered with the first dose or not. Therefore, the leakage of Gd-DTPA from the Gd-liposomes will not influence this study. In addition, many studies demonstrated that ABC phenomenon for empty liposome was observed determined by [H^3]-labelled or ^{99m}Tc-labelled method (5–9).

It is believed that macrophages in the RES play an important role in ABC, and liposomes were mainly located in Kupffer cells after a second injection (5,8).When hepatosplenic macrophages were depleted, no enhanced clearance of liposomes was observed (6). The induction of ABC with liposomes could be attributable to a 150 kDa serum factor (5), anti-PEG IgM (9,11,12,22,23), anti-PEG antibody (10), or anti-PEG IgG antibody (24).

Whereas the mechanism of the immune response on repeated injections of liposomes has not been fully elucidated yet, the enhanced clearance effect can still be divided into two phases: the induction phase following the first injection and the effectuation phase following the second injection (6). According to this theory, there are two very important factors: one is the biological material (e.g. antibody) produced in the induction phase, the other is the recognition of the antibody by the second dose. For the effectuation phase, it was reported that the ABC phenomenon was induced by the second dose of a PEGylated liposome, but not of a liposome lacking a PEG-coating (23). This indicates that PEG is essential for the nanocarrier to recognize the antibody in the effectuation phase. In this study, the ABC phenomenon was not observed after repeated injections of the Gd-micelle at different doses and time intervals. This ABC failure of Gd-micelle may be caused by the failure for the production of biological material in the induction phase (data not shown) or/and for the recognization by the antibody in the effectuation phase. Even if the first injection was of empty liposome, the second injection of the Gd-micelle did not produce the ABC phenomenon either. This suggests that the antibody produced by the empty liposome in the induction phase is not recognized by the PEG moiety of the Gd-micelle. Therefore, not only PEG, but also other factors such as structure and hydrophobic character affect recognition.

For the induction phase, the ABC phenomenon was not observed when the amount of PEGylated lipid of liposomes in the first injection was more than 10 mol% (7,8). We have previously reported the accelerated clearance of [^{3}H]-labeled PEGylated liposomes in mice pre-administered empty PEG-PBLA polymeric micelles (16). Furthermore, repeated

injections of PEG-PLA nanoparticles also produced the ABC phenomenon (12). Hence, the structure and component of nanocarriers has a considerable impact on the induction phase of ABC. From a structural perspective, the Gd-micelle formed through ionic interactions; therefore, it does not have any hydrophobic part (Fig. 1). In contrast, the PEG-PBLA micelle is composed of both a hydrophilic part, PEG, and a hydrophobic part, PBLA. Similarly, PEGylated liposomes possess a hydrophilic PEG chain and a hydrophobic bilayer membrane. The immunogenicity of an antigen can be affected by factors such as the physical and chemical properties of the antigen, its dose, and so on (25). The reasons why the Gd-micelle evaded the ABC phenomenon have not yet been elucidated at the present stage. The absence of a hydrophobic part may be a key for this elucidation because the other ABC-phenomenon-positive PEG-based carrier systems possess hydrophobic part in a hydrophobic inner core for polymeric micelles and in a lipid bilayer for PEG-liposomes. We are currently investigating the ABC phenomenon induced by other kinds of polymeric micelles and nanoparticles. It is hoped that these experiments will provide more evidence for the mechanism of the ABC phenomenon.

CONCLUSIONS

The Gd-micelle did not induce ABC following its pre-administration at various doses and time intervals. In contrast, the Gd-liposome induced the phenomenon when it or an empty PEGylated liposome, but not the $PEG_{500,000}$ macromolecule or PEG_{2000}-DSPE, was pre-administered. ABC-phenomenon-positive PEG-based carrier systems possess a hydrophobic part in a hydrophobic inner core for polymeric micelles and in a lipid bilayer for PEG-liposomes. The absence of a hydrophobic part of Gd-micelle may be a key factor for not producing the ABC phenomenon.

ACKNOWLEDGMENTS

This study was supported by the Ministry of Health, Labour, and Welfare of Japan. We also acknowledge the support from the Program for Promoting the Establishment of Strategic Research Centers, Special Coordination Funds for Promoting Science and Technology and the Ministry of Education, Culture, Sports, Science and Technology of Japan.

REFERENCES

1. Allen TM, Hansen C, Martin F, Redemann C, Yau-Young A. Liposomes containing synthetic lipid derivatives of poly(ethylene glycol) show prolonged circulation half-lives *in vivo*. Biochim Biophys Acta. 1991;1066:29–36.
2. Woodle MC, Lasic DD. Sterically stabilized liposomes. Biochim Biophys Acta. 1992;1113:171–99.
3. Lasic DD, Martin FJ, Gabizon A, Huang SK, Papahadjopoulos D. Sterically stabilized liposomes: a hypothesis on the molecular origin of the extended circulation times. Biochim Biophys Acta. 1991;1070:187–92.
4. Torchilin VP, Omelyanenko VG, Papisov MI, Bogdanov AA Jr, Trubetskoy VS, Herron JN, *et al.* Poly(ethylene glycol) on the liposome surface: on the mechanism of polymer-coated liposome longevity. Biochim Biophys Acta. 1994;1195:11–20.
5. Dams ET, Laverman P, Oyen WJ, Storm G, Scherphof GL, van Der Meer JW, *et al.* Accelerated blood clearance and altered biodistribution of repeated injections of sterically stabilized liposomes. J Pharmacol Exp Ther. 2000;292:1071–9.
6. Laverman P, Carstens MG, Boerman OC, Dams ET, Oyen WJ, van Rooijen N, *et al.* Factors affecting the accelerated blood clearance of polyethylene glycol-liposomes upon repeated injection. J Pharmacol Exp Ther. 2001;298:607–12.
7. Ishida T, Ichikawa T, Ichihara M, Sadzuka Y, Kiwada H. Effect of the physicochemical properties of initially injected liposomes on the clearance of subsequently injected PEGylated liposomes in mice. J Control Release. 2004;95:403–12.
8. Ishida T, Harada M, Wang XY, Ichihara M, Irimura K, Kiwada H. Accelerated blood clearance of PEGylated liposomes following preceding liposome injection: effects of lipid dose and PEG surface-density and chain length of the first-dose liposomes. J Control Release. 2005;105:305–17.
9. Ishida T, Kiwada H. Accelerated blood clearance (ABC) phenomenon upon repeated injection of PEGylated liposomes. Int J Pharm. 2008;354:56–62.
10. Judge A, McClintock K, Phelps JR, Maclachlan I. Hypersensitivity and loss of disease site targeting caused by antibody responses to PEGylated liposomes. Mol Ther. 2006;13:328–37.
11. Semple SC, Harasym TO, Clow KA, Ansell SM, Klimuk SK, Hope MJ. Immunogenicity and rapid blood clearance of liposomes containing polyethylene glycol–lipid conjugates and nucleic acid. J Pharmacol Exp Ther. 2005;312:1020–6.
12. Lu W, Wan J, She ZJ, Jiang XG. Brain delivery property and accelerated blood clearance of cationic albumin conjugated pegylated nanoparticle. J Control Release. 2007;118:38–53.
13. Gabizon A, Isacson R, Rosengarten O, Tzemach D, Shmeeda H, Sapir R. An open-label study to evaluate dose and cycle dependence of the pharmacokinetics of pegylated liposomal doxorubicin. Cancer Chemother Pharmacol. 2008;61:695–702.
14. Kakizawa Y, Kataoka K. Block copolymer micelles for delivery of gene and related compounds. Adv Drug Deliv Rev. 2002;54:203–22.
15. Yokoyama M, Okano T, Sakurai Y, Ekimoto H, Shibazaki C, Kataoka K. Toxicity and antitumor activity against solid tumors of micelle-forming polymeric anticancer drug and its extremely long circulation in blood. Cancer Res. 1991;51:3229–36.
16. Koide H, Asai T, Hatanaka K, Urakami T, Ishii T, Kenjo E, *et al.* Particle size-dependent triggering of accelerated blood clearance phenomenon. Int J Pharm. 2008;362:197–200.
17. Lin SP, Brown JJ. MR contrast agents: physical and pharmacologic basics. J Magn Reson Imaging. 2007;25:884–99.
18. Mulder WJ, Strijkers GJ, van Tilborg GA, Griffioen AW, Nicolay K. Lipid-based nanoparticles for contrast-enhanced MRI and molecular imaging. NMR Biomed. 2006;19:142–64.
19. Shiraishi K, Kawano K, Minowa T, Maitani Y, Yokoyama M. Preparation and in vivo imaging of PEG-poly(L-lysine)-based polymeric micelle MRI contrast agents. J Control Release. 2009;136:14–20.
20. Nakamura E, Makino K, Okano T, Yamamoto T, Yokoyama M. A polymeric micelle MRI contrast agent with changeable relaxivity. J Control Release. 2006;114:325–33.
21. Wang XY, Ishida T, Ichihara M, Kiwada H. Influence of the physicochemical properties of liposomes on the accelerated blood clearance phenomenon in rats. J Control Release. 2005;104:91–102.
22. Ishida T, Ichihara M, Wang XY, Yamamoto K, Kimura J, Majima E, *et al.* Injection of PEGylated liposomes in rats elicits PEG-specific IgM, which is responsible for rapid elimination of a second dose of PEGylated liposomes. J Control Release. 2006;112:15–25.
23. Wang XY, Ishida T, Kiwada H. Anti-PEG IgM elicited by injection of liposomes is involved in the enhanced blood clearance of a subsequent dose of PEGylated liposomes. J Control Release. 2007;119:236–44.
24. Sroda K, Rydlewski J, Langner M, Kozubek A, Grzybek M, Sikorski AF. Repeated injections of PEG-PE liposomes generate anti-PEG antibodies. Cell Mol Biol Lett. 2005;10:37–47.
25. Abbas AK, Lichtman AH, Pober JS. Cellular and molecular immunology. Philadelphia: Saunder; 1991.

Langmuir
Article
pubs.acs.org/Langmuir

Encapsulation of a Hydrophobic Drug into a Polymer-Micelle Core Explored with Synchrotron SAXS

Isamu Akiba,* Naotaka Terada, Satoshi Hashida, and Kazuo Sakurai*

Department of Chemistry and Biochemistry, The University of Kitakyushu, 1-1 Hibikino, Kitakyushu 808-0135, Japan

Taku Sato, Kouichi Shiraishi, and Masayuki Yokoyama

Research Center for Medical Science, Jikei University School of Medicine, 3-25-8 Nishi-Shinbashi, Minato-ku, Tokyo 105-8461, Japan

Hiroyasu Masunaga,† Hiroki Ogawa,† Kazuki Ito,‡ and Naoto Yagi†

†*Japan Synchrotron Radiation Research Institute (JASRI/SPring-8), 1-1-1 Kouto, Sayo 679-5198, Japan, and* ‡*Structural Science Laboratory, RIKEN SPring-8, 1-1-1 Kouto, Sayo 679-5198, Japan*

Received November 17, 2009. Revised Manuscript Received January 30, 2010

Synchrotron small-angle X-ray scattering (SAXS) at the SPring-8 40B2 and 45XU beamlines was carried out on aqueous solutions of (PEG-P(Asp(Bzl))): partially benzyl-esterified poly(ethylene glycol)-*block*-poly(aspartic acid) with LE540 loaded up to 8.3 wt %, where LE540 is a very hydrophobic retinoid antagonist drug. The scattering profiles showed characteristic features for core−shell spherical micelles, confirming that P(Asp(Bzl)) forms a hydrophobic core and PEG forms a hydrophilic shell. Before the addition of LE540, a diffraction peak was observed around $q = 4$ nm^{-1}, where q is the magnitude of the scattering vector. This peak can be attributed to ordering between α-helices made of P(Asp(Bzl)), the so-called nonspecific hexatic arrangement. The P(Asp(Bzl)) helices disappeared as LE540 was added. This result can be interpreted by assuming a uniform distribution of LE540 in the core. By use of a core−shell spherical micelle model, the SAXS data could be well fitted for all of the samples. The analysis indicated that the core radius increases sigmoidally from 5.9 to 6.9 nm upon addition of LE540 whereas the shell radius stayed at 12.5−12.8 nm. The aggregation number that is the average number of PEG-P(Asp(Bzl))'s consisting of one micelle slightly increased from 145 to 182.

1. Introduction

Amphiphilic block copolymers can self-assemble into a spherical micelle with core−shell architecture in aqueous solutions. Here, the hydrophobic blocks are segregated from water to form a densely packed core that can encapsulate hydrophobic compounds, and the hydrophilic blocks can be dissolved in water and thus form a diffuse, soft interface with water.[1] These micelles are called polymeric micelles and are expected to play an important role in drug delivery systems (DDSs) in the future.[2−4] This is because the soft interface provides a stealth effect to prolong blood circulation and the core can transport hydrophobic drugs.[5] In fact, several polymeric micelles incorporating anticancer drugs are under clinical evaluation[6−11] and fall into the category of biocompatible copolymers consisting of poly(ethylene glycol) (PEG) and hydrophobic polypeptides such as poly(aspartic acid) derivatives and poly(glutamic acid) derivatives. The main reason and the main advantage are that they are nontoxic and induce less immunological response after being injected into living bodies.

In terms of designing DDS particles, increasing the drug-loading rate and controlling the release profile are critical issues and are considered to be related to how the drug molecules are encapsulated and distributed in the core. Although its importance has been noticed, there is no in situ technique to observe the drugs in the core directly. Yamamoto et al.[12] made an attempt to clarify a key parameter to induce the incorporation and stabilization of hydrophobic drugs in the core. By use of a fluorescent probe, they evaluated the hydrophobicity of the core and compared it with the compatibility between the core and the drugs. They pointed out the importance of an adequate balance between the core hydrophobicity and the configuration of the hydrophobic block; however, they did not seem to have reached a final conclusion. There have been many microscopy studies on the morphology of polymeric micelles, including cryo-TEM.[13,14] However, even

*Corresponding authors. E-mail: akiba@env.kitakyu-u.ac.jp (I.A.), sakurai@env.kitakyu-u.ac.jp (K.S.).

(1) Zhang, L. F.; Eisenberg, A. *Science* **1995**, *268*, 1728–1731.
(2) Aliabadi, M.; Lavasanifar, A. *Expert Opin. Drug Delivery* **2006**, *3*, 139–162.
(3) Kwon, G. S. *Crit. Rev. Ther. Drug Carrier Syst.* **2003**, *20*, 357–403.
(4) Yokoyama, M. In *Polymeric Drug Delivery Systems*; Kwon, G. S., Ed.; Drugs and the Pharmaceutical Sciences; Taylor & Francis: Boca Raton, FL, 2005; Vol. *148*.
(5) Yokoyama, M.; Okano, T.; Sakurai, Y.; Fukushima, S.; Okamoto, K.; Kataoka, K. *J. Drug Targeting* **1999**, *7*, 171–186.
(6) Negishi, T.; Koizumi, F.; Uchino, H.; Kuroda, J.; Kawaguchi, T.; Naito, S.; Matsumura, Y. *Br. J. Cancer* **2006**, *95*, 601–606.
(7) Nakajima, T.; Yanagihara, K.; Takigahira, M.; Yasunaga, M.; Kato, K.; Hamaguchi, T.; Yamada, Y.; Shimada, Y.; Mihara, K.; Ochiya, T.; Matsumura, Y. *Cancer Res.* **2008**, *68*, 9318–9322.
(8) Matsumura, Y. *Adv. Drug Delivery Rev.* **2008**, *60*, 899–914.
(9) Nishiyama, N.; Okazaki, S.; Cabral, H.; Miyamoto, M.; Kato, Y.; Sugiyama, Y.; Nishio, K.; Matsumura, Y.; Kataoka, K. *Cancer Res.* **2003**, *63*, 8977–8983.
(10) Uchino, H.; Matsumura, Y.; Negishi, T.; Koizumi, F.; Hayashi, T.; Honda, T.; Nishiyama, N.; Kataoka, K.; Naito, S.; Kakizoe, T. *Br. J. Cancer* **2005**, *93*, 678–387.
(11) Nakanishi, T.; Fukushima, S.; Okamoto, K.; Suzuki, M.; Matsumura, Y.; Yokoyama, M.; Okano, T.; Sakurai, Y.; Kataoka, K. *J. Controlled Release* **2001**, *74*, 295–302.
(12) Yamamoto, T.; Yokoyama, M.; Opanasopit, P.; Hayama, A.; Kawano, K.; Maitani, Y. *J. Controlled Release* **2007**, *123*, 11–18.
(13) Zupancich, J. A.; Bates, F. S.; Hillmyer, M. A. *Biomacromolecules* **2009**, *10*, 1554–1563.
(14) Bhargava, P.; Zheng, J. X.; Li, P.; Quirk, R. P.; Harris, F. W.; Cheng, S. Z. D. *Macromolecules* **2006**, *39*, 4880–4888.

these most elaborate techniques seem to fail to observe how the drugs are incorporated into the core.

Small-angle scattering is a powerful tool for determining the size, shape, and internal structures of nanosized particles in solution.[15−23] Riley et al.[21] were the first to study small-angle neutron scattering (SANS) from DDS polymer micelle solutions made from poly(lactic acid)-*b*-poly(ethylene glycol) (PLA-*b*-PEG) and accurately determined the inner structure of the micelle. They found that the shell thickness and the PEG block conformation are strongly correlated with the PLA core size: the PEG segments are localized in the vicinity of the PLA/PEG interface in the smaller core; in contrast, they became more homogeneous along the radial direction in the case of the larger core. Although those micelles are not used as DDSs, several groups studied them with SANS and/or SAXS (small-angle X-ray scattering)[19,22,24] and revealed that these techniques are useful for in situ measurements of the polymeric micelle. Recently, Bhattacharjee et al.[25] measured SANS from poly(ethylene oxide)−poly(propylene oxide)−poly(ethylene oxide) triblock copolymers (pluronic P123) encapsulating the anticancer drug doxorubicin hydrochloride and found that there was no appreciable change in the core size upon drug loading. As Yamamoto et al.[12] noticed, the more hydrophobic the drug that is loaded, the more changes that occur in the micellar properties. For this reason, we used LE540 (a very hydrophobic retinoid antagonist drug, see Scheme 1 for the chemical structure) as a model drug in this study.

We have constructed a bespoke SAXS chamber that enables a sample or scattering cell to be set in vacuum and a vacuum-proof solution cell with 0.20-mm-thick quartz windows. Combining these two instruments, we improved the S/N ratio by almost 10 times over the entire q range and drastically eliminated parasitic scattering near beam stoppers compared with conventional setups.[26] Furthermore, the top-up operation at SPring-8 provided an extremely stable X-ray flux. These conditions enabled us to determine the absolute scattering intensity and thus the molecular weight of the scattering objects more accurately than ever (see the Supporting Information). With these advantages, this article presents synchrotron SAXS studies on the PEG-P(Asp(Bzl)) micelle containing a small amount of LE540, where (PEG-P(Asp(Bzl))) is partially benzyl-esterified poly(ethylene glycol)-*block*-poly(aspartic acid) and is now under clinical evaluation in Japan.

2. Experimental Section

Materials. PEG-P(Asp(Bzl)) represented in Scheme 1a was used in this study. The synthesis of PEG-P(Asp(Bzl)) was carried out by ring-opening polymerization of benzyl *L*-aspartate *N*-carboxyanhydride from a primary amino-terminated PEG, followed by partial esterification of the side chains with benzyl bromide after removal of the benzyl groups, as described elsewhere.[12,27] The poly(amino acid) block was composed of a 1:3 (mol/mol) mixture of the α-amide and β-amide aspartic acid residues resulting from an alkaline hydrolysis procedure in block copolymer synthesis. Benzyl ester was formed at 76% of the aspartic acid residues, and the other 24% of the residues were unmodified aspartic acids. The number-average molecular weights of PEG and P(Asp(Bzl)) blocks were determined to be 5.2×10^3 and 4.6×10^3 g/mol, respectively. The characterization of PEG-P(Asp(Bzl)) was described in detail in previous studies.[12,27] LE540 (Scheme 1b), which is a retinoid antagonist,[28,29] was used as a hydrophobic drug compound. It was purchased from Wako Pure Chemicals Industry, Japan. On the basis of its solubility test,[29] LE540 essentially does not dissolve in water at all, thus all of the loaded LE540 molecules are supposed to be incorporated into the P(Asp(Bzl)) hydrophobic core.

Scheme 1

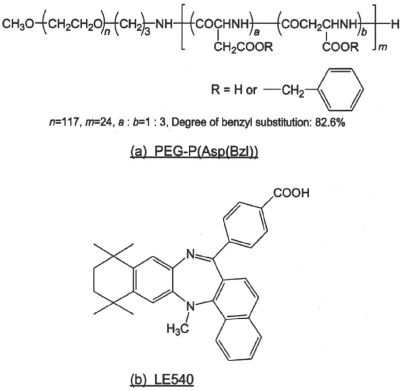

Sample Preparation. PEG-P(Asp(Bzl)) and LE540 were dissolved in THF at a desired loading ratio (denoted L_{LE540}), and then THF was evaporated at 45 °C under N_2 flow. The PEG-P(Asp(Bzl))/LE540 mixtures were further dried under reduced pressure and then dispersed in 1× Dulbecco buffer at 25 mg/mL, and the solution was ultrasonicated for a few minutes. The solutions were diluted to the desired concentration with the buffer, and the concentration of the micelle including LE540 is denoted by C_M. The hydrodynamic diameters (R_H) of the micelles were measured by dynamic light scattering with a Malvern Zetasizer Nano (Malvern, U.K.) and are listed in Table 1. In the case of $L_{LE540} < 9\%$, no precipitation was observed after the dissolution of PEG-P(Asp(Bzl)) and LE540. Therefore, we decided to keep L_{LE540} at less than 8.5%.

Synchrotron SAXS Measurements. SAXS measurements were performed at BL-40B2 and BL-45XU at SPring-8, Japan. A 30 cm × 30 cm imaging plate (Rigaku R-AXIS VII) detector was placed 0.75 or 4.0 m away from the sample. The wavelength of the incident beam (λ) was 0.10 nm. The 0.75 and 4.0 m setups

(15) Glatter, O.; Scherf, G.; Shillen, K.; Brown, W. *Macromolecules* **1994**, *27*, 6046–6054.
(16) Svergun, D. I. *J. Appl. Crystallogr.* **2000**, *33*, 530–534.
(17) Feigin, L. A.; Svergun, D. I. *Structure Analysis by Small-Angle X-ray and Neutron Scattering*; Plenum Press: New York, 1987.
(18) Roe, R.-J. *Methods of X-ray and Neutron Scattering in Polymer Science*; Oxford University Press: New York, 2000.
(19) Hickel, P.; Ballauff, M.; Jada, A. *Macromolecules* **1996**, *29*, 4006–4014.
(20) Dupty, C.; Auvray, X.; Petipas, C.; Anthore, R. *Langmuir* **1996**, *12*, 3162–3172.
(21) Riley, T.; Heald, C. R.; Stolnik, S.; Garnett, M. C.; Illum, L.; Davis, S. S.; King, S. M.; Heenan, R. K.; Purkiss, S. C.; Barlow, R. J.; Gellert, P. R.; Washington, C. *Langmuir* **2003**, *19*, 8428–8435.
(22) Nakano, M.; Deguchi, M.; Matsumoto, K.; Matsuoka, H.; Yamaoka, H. *Macromolecules* **1999**, *32*, 7437–7443.
(23) He, L.; Garamus, V. M.; Funari, S. S.; Malfois, M.; Willumeit, R.; Niemeyer, B. *J. Phys. Chem. B* **2002**, *106*, 7696–7604.
(24) Pedersen, J. S.; Svaneborg, C.; Almdal, K.; Hamley, I. W.; Young, R. N. *Macromolecules* **2003**, *36*, 416–433.
(25) Bhattacharjee, J.; Verma, G.; Aswal, V. K.; Hassan, P. A. *Pramana* **2008**, *71*, 991–995.
(26) Sakuragi, M.; Kusuki, S.; Hamada, E.; Masunaga, H.; Ogawa, H.; Akiba, I.; Sakurai, K. *J. Phys. Conf. Ser.* **2009**, *184*, 012008.
(27) Yokoyama, M.; Opanasopit, P.; Okano, T.; Kawano, K.; Maitani, Y. *J. Drug Targeting* **2004**, *12*, 373–384.
(28) Li, Y.; Hashimoto, Y.; Agadir, A.; Kagechika, H.; Zhang, X.-k. *J. Biol. Chem.* **1999**, *274*, 15360–15366.
(29) Umemiya, H.; Fukasawa, H.; Ebisawa, M.; Eyrolles, L.; Kawachi, E.; Eisenmann, G.; Gronemeyer, H.; Hashimoto, Y.; Shudo, K.; Kagechika, H. *J. Med. Chem.* **1997**, *40*, 4222–4234.

Table 1. Characteristics of PEG-P(Asp(Bzl))/LE540 Micelles

LE540 content/ wt % for PEG-P(Asp(Bzl))[a]	D_H/nm[b]	R_g/nm[c]	R_g/R_H[b]	$I(0)$/cm^{-1}[c]	$\bar{\rho} - \rho_0$/e/nm^3
0	24	6.46	0.54	0.012	23.0
1.4	23	6.46	0.56	0.013	23.0
3.0	24	6.28	0.52	0.014	22.9
5.8	28	6.53	0.41	0.014	22.8
8.3	25	6.82	0.55	0.014	22.6

[a]LE540 contents were determined by UV−vis spectroscopy. [b]Hydrodynamic diameters (D_H) and hydrodynamic radii (R_H) were determined by dynamic light scattering with cumulant analyses. [c]R_g and $I(0)$ were determined by Guinier analyses.

provided q ranges of 2.0−8.0 and 0.05−2.0 nm^{-1}, respectively, where q is the magnitude of the scattering vector ($q = (4\pi/\lambda) \sin\theta$, where 2θ is the scattering angle), and the former range corresponds to a length scale of 0.8−3.1 nm in real space and the latter corresponds to a length scale of 3.1−125 nm. As mentioned in the Introduction, a bespoke SAXS vacuum sample chamber[26] was used and the X-ray transmittance of a sample was determined with an ion chamber located in front of the sample and a Si photodiode was used for X-rays (Hamamatsu Photonics S8193) after the sample.

A micelle solution was packed in a quart capillary (2 mm Φ, Hilgenberg GmbH) or our special cell (Supporting Information) and set in the sample chamber. SAXS from a sample solution was measured at an exposure time of 5 or 10 min. The resulting 2D SAXS images were converted to 1D $I(q)$ versus q profiles by circular averaging. Here, $I(q)$ was the scattering intensity at q, and to obtain the excess scattering intensity $I(q)$ by micelles, the scattering from the background due to the buffer, the cell, and density fluctuations was subtracted. Here, density fluctuations were determined by the fitting of the scattering profiles over $4 < q < 8$ nm^{-1} with the empirical equation proposed by Ruland.[30] The measured SAXS intensities were corrected to an absolute scale using the absolute scattering intensities of water and ovalbumine (Supporting Information).[17,31]

The scattering experimets were carried out at $C_M = 1.25$ mg/mL for most of the samples. To examine the dense packing effect due to high concentration, we measured $C_M = 0.625$, 1.25, 2.5, and 25 mg/mL for $L_{LE540} = 0$.

3. Theoretical Background for SAXS Data Analysis

The SAXS intensity from solutions containing identical and randomly oriented particles may be expressed by[32]

$$I(q) = NV_M^2(\bar{\rho} - \rho_0)^2 P(q)\, S(q) \tag{1}$$

where N is the number of particles in a unit volume, V_M is the particle volume, ρ_0 and $\bar{\rho}$ are the scattering-length densities (or electron densities) of the solvent and the particle, respectively. When the particle has an inhomogeneous inner structure, $\bar{\rho}$ is given by taking an average over all particles. $P(q)$ is the form factor of the particle, and $S(q)$ is the structure factor. $P(q)$ reflects the inner structure of the particle (i.e., internal electron density distribution) and the overall shape. Because $S(q)$ describes the interparticle interference, when the interference between particles is negligibly small and/or for relatively high q, the relation of $S(q) \approx 1$ can be held. In the present samples, we observed interparticle interference at $q < 0.5$ nm^{-1} for $C_M = 2.5$ mg/mL, but there was no such interference observed for the lower concentrations ($C_M \leq 1.25$ mg/mL) and $I(q)/C$ was constant over the entire range as presented in the Supporting Information.

The forward scattering intensity $I(0)$ can be written as

$$I(0) = NV_M^2(\bar{\rho} - \rho_0)^2 = \frac{M_M}{N_A} C_M \bar{\nu}^2(\bar{\rho} - \rho_0)^2 \tag{2}$$

where N_A is Avogadro's number and $\bar{\nu}$ is the partial specific volume of a micelle and can be related to the isothermal compressibility. For static light scattering, the magnitude of $\bar{\nu}^2(\bar{\rho} - \rho_0)^2$ can be directly determined as the differential index of refraction of the solute. In the case of SAXS, however, the terms $\bar{\nu}$ and $\bar{\rho} - \rho_0$ have to be given separately. Here, $\bar{\rho} - \rho_0$ can be calculated from the atomic scattering factor.[18] When scattering objects are homogeneous (such as homopolymer chains or polymer latexes), the bulk density can be a good approximation of $\bar{\nu}$. However, when scattering objects are inhomogeneous, such as multilayer micelles or copolymers, we cannot use such an approximation. Because $\bar{\nu}$ is a thermodynamic value, it has to be determined independently.

In the present work, the micellar shapes are described by core−shell spheres given by the following expression:

$$I(q) = NV_S^2\left\{(\rho_C - \rho_S)\frac{V_C}{V_S}\frac{3[\sin(qR_C) - qR_C\cos(qR_C)]}{(qR_C)^3} + (\rho_S - \rho_0)\frac{3[\sin(qR_S) - qR_S\cos(qR_S)]}{(qR_S)^3}\right\}^2 \tag{3}$$

Here, R_C and R_S are the outer radii of the core and shell and ρ_C and ρ_S are the scattering lengths (or electron densities) of the core and the shell, respectively. In this model, ρ_C and ρ_S can be related to $\bar{\rho}$ in eq 2 through the following relations by the use of $R_S = R$ and $V_M = (4\pi/3)R^3$:

$$\bar{\rho} = \frac{V_C\rho_C + (V_S - V_C)\rho_S}{V_S} = \phi_C\rho_C + (1 - \phi_C)\rho_S \tag{4}$$

Here, $\phi_C = (R_C/R_S)^3$. For this model, the radius of gyration R_g in the Guinier law can be given by

$$R_g^2 = \frac{3[V_C R_C^2(\rho_C - \rho_S) + V_S R_S^2\rho_S]}{5[V_C(\rho_C - \rho_S) + V_S\rho_S]} \tag{5}$$

In our analysis, R_g was determined first from the Guinier plot and subsequently R_C, R_S, and ρ_S were determined so as to satisfy eq 5 under the restricting conditions that $R_C < R_S$ and ρ_S and ρ_C take reasonable values in terms of the molecular structures.

4. Results and Discussion

SAXS Profiles and General Results. Figure 1 plots $I(q)$ against q in the range of 0.07 nm$^{-1} < q < 2$ nm^{-1} for PEG-P(Asp(Bzl)) micelles at $L_{LE540} = 0$, 1.4, 3.0, 5.8, and 8.3 wt %, and the profiles for $0.07 < q < 0.1$ nm^{-1} are magnified in the inset. The q range in this Figure should reflect the micelle size and its inner structures. All SAXS profiles converge to a plateau at a smaller $q = 0.07$−0.4 nm^{-1}, confirming that PEG- P(Asp(Bzl)) and the drug-loaded ones indeed formed an isolated micelle. The profiles showed the secondary maximum at $q \approx 0.9$ nm^{-1}, suggesting that the micelles had a well-defined structure with a relatively narrow size distribution. There was a minimum or shoulder around $q = 0.7$−0.8 nm^{-1}, indicating that the radius of the particle is about 6.1−5.6 nm as estimated from the relation

(30) Ruland, W. *Colloid Polym. Sci.* **1977**, *255*, 417–427.
(31) Orthaber, D.; Bergmann, A.; Glatter, O. *J. Appl. Crystallogr.* **2000**, *33*, 218–225.
(32) Pedersen, J. S. In *Neutrons, X-rays and Light: Scattering Methods Applied to Soft Condensed Matter*; Lindner, P., Zemb, T., Eds.; Elsevier: Amsterdam, 2002.

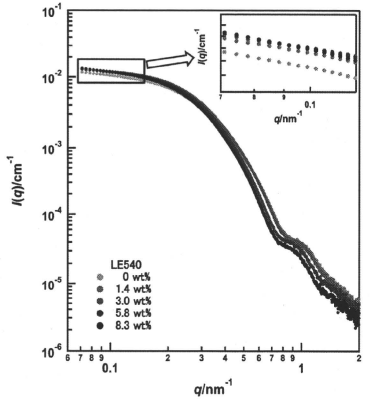

Figure 1. SAXS profile changes for the PEG-P(Asp(Bzl)) micelle upon LE540 loading. The inset magnifies the low-q region, and the ordinates axis is the absolute X-ray intensity. The concentration of the samples is 1.25 mg/mL.

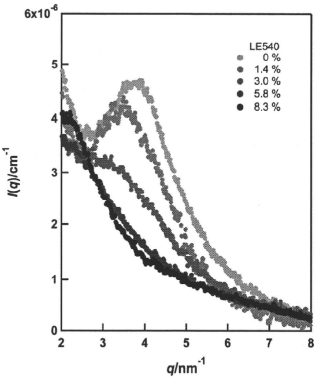

Figure 2. Magnified linear−linear plot in the range of 2 nm^{-1} < q < 8 nm^{-1} to show the presence of ordering due to hexagonal chains of P(Asp(Bzl)) and the disappearance upon addition of LE540.

$Rq^* = 4.493$ for solid spheres, where q^* is the minimum position and R is the radius of the solid sphere. With increasing L_{LE540}, the SAXS profiles were shifted to lower q. This feature can be interpreted as the expansion of micelle size upon incorporation of LE540, presumably into the core. The absolute values of $I(q)$ at lower q increased with increasing L_{LE540}. This increment can be explained if the added LE540 simply increased the scattering volume V_M and/or the average electron density of $\bar{\rho}$ (eq 2).

Figure 2 shows the SAXS profiles at 2 nm^{-1} < q < 8 nm^{-1}, corresponding to 0.4−3 nm in real space. The micelles at L_{LE540} = 0 and 1.4 wt % exhibited a clear diffraction peak at $q \approx 4$ nm^{-1}. According to the bulk poly(β-benzyl-L-aspartate) (PBLA) data,[33] this peak can be attributed to ordering between the helices made from P(Asp(Bzl)) chains, called nonspecific hexatic arrangement.[33] The diffraction peak becomes drastically weaker with increasing L_{LE540} and eventually disappears. The decrease in the peak intensity corresponds to a decrease in the ordering of the P(Asp(Bzl)) helices. This phenomenon can be interpreted as a uniform distribution of LE540 in the P(Asp(Bzl)) core, and the interaction between LE540 and P(Asp(Bzl)) is more favorable than the helix formation of P(Asp(Bzl)).

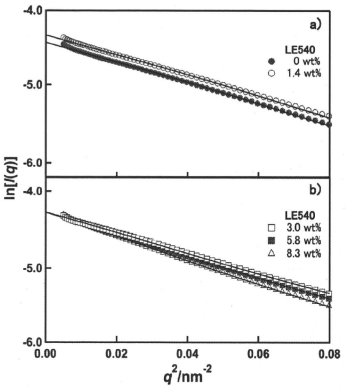

Figure 3. Guinier plots for the PEG-P(Asp(Bzl)) micelle with LE540 contents of (a) 0 and 1.4 wt % and (b) 3.0, 5.8, and 8.3 wt %.

Guinier Analysis. The Guinier law[17] is given by the following equation:

$$I(q) = I(0)\exp(-q^2R_g^2/3) \quad (6)$$

According to the eq 6, $I(0)$ and R_g are obtained from the intercept and the slope of the ln[$I(q)$] versus q^2 plot (Guinier plot). As shown in Figure 3, the Guinier plot accurately determined the sets of $I(0)$ and R_g within an experimental error of 3%, and the data are listed in Table 1. When we divided R_g by R_H in the fourth column in Table 1, it could be found that $R_g/R_H \approx 0.5$ for all samples and that these values are lower than that of hard spheres ($R_g/R_H = (3/5)^{1/2} = 0.775$ if R_H can be considered to be its radius). This fact suggests that the micelle has a larger electron-density portion in its inner space,[34] and such architecture can be well represented by a core−shell spherical model. Furthermore, the results show that R_g/R_H was almost independent of L_{LE540}. If the original shape at $L_{LE540} = 0$ was deformed anisotropically, such as from spherical to ellipsoidal or a rodlike shape, then the R_g/R_H ratio would not be constant. Therefore, it is suggested that the spherical shape of the micelle is not changed upon LE540 loading. Figure 4 shows a plot of $I(0)$ and R_g against L_{LE540}. With increasing L_{LE540} from 0 to 3%, $I(0)$ increased from 0.012 to 0.014 cm^{-1} and stayed at 0.014 cm^{-1} in the range of $L_{LE540} > 3$. R_g did not change at $L_{LE540} < 3$ and increased from 6.4 to 6.8 nm with an increase in L_{LE540} from 3 to 8.3%. According to eq 2, $I(0)$ is proportional to $V_M^2(\bar{\rho} - \rho_0)^2$. Because R_g increased upon

(33) Tanaka, S.; Ogura, A.; Kaneko, T.; Murata, Y.; Akashi, M. *Macromolecules* **2004**, *37*, 1370–1377.

(34) Antonietti, M.; Bremser, W.; Schmidt, M. *Macromolecules* **1990**, *23*, 3796–3805.

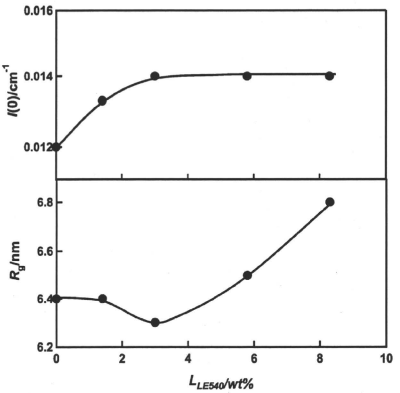

Figure 4. L_{LE540} dependence of $I(0)$ and R_g.

adding L_{LE540}, V_M also increased accordingly. Therefore, the constant $I(0)$ in the range of $L_{LE540} > 3$ means that $\bar{\rho}$ decreased with increasing L_{LE540}. This is consistent with the relation between the electron density of LE540 and P(Asp(Bzl)) ($\rho_{LE540} < \rho_{P(Asp(Bzl))}$); therefore, $\bar{\rho}$ decreased upon the addition of LE540, which has a lower density.

Analysis with the Core−Shell Model at $L_{LE540} = 0$. To evaluate the inner structure, we used a spherical core−shell model given by eq 3. At $L_{LE540} = 0$, the core is composed of only P(Asp(Bzl)) and thus ρ_C can be evaluated to be 489 e/nm^3 by combining the bulk density of P(Asp(Bzl)) (ca. 1.30 g cm^{-3}) with its chemical structure.[35] Because we used the solvent as water, we chose ρ_0 = 334 e/nm^3. The electron density of PEG in the amorphous state is 369 e/nm^3.[36] Because the PEG blocks are dissolved in water, ρ_S must take a value between 334 and 369 e/nm^3. These are the constraining conditions for ρ_0, ρ_S, and ρ_C. Furthermore, the two geometrical parameters R_C and R_S have to satisfy eq 5 with R_g = 6.4 nm and are restricted by $R_C < R_S$. Under these constraining conditions, ρ_S is regarded to be a function of R_C and R_S (Supporting Information Figure S4). Therefore, we can perform the fitting analysis to the SAXS profile by the use of only two adjustable parameters of R_C and R_S.

Figure 5a,b compares the experimental data and the calculations. Panel a compares three different combinations with the same R_S. As expected, all three curves well reproduced the Guinier region (indicated by the dotted line, $qR_g < 1.0$). Outside of this region, the calculated lines deviated from the data. Panel b compares three different combinations with the same R_C. In this case, ρ_C is uniquely determined by R_S. By iterating these processes, we found that the combination of R_C = 5.9 nm, R_S = 12.5 nm, and ρ_S = 340 e/nm^3 can provide the best-fit curve. Finally, we took the size distribution into account. We assumed that the size distribution can be described by the Gaussian function[22]

$$P(R) = \frac{1}{\sqrt{2\pi}\sigma}\exp\left[-\frac{(R-R_0)^2}{2\sigma^2}\right] \quad (7)$$

where R_0 and σ are the average radius of the micelle and the standard deviation of micelle size, respectively. Figure 6 shows the final fitting results. The calculated curve became smeared with increasing polydispersity (σ/R_0) and eventually agreed with the experimental data at $\sigma/R_0 = 0.15$, except for $q > 1.2$ nm^{-1} where the ordering of the P(Asp(Bzl)) chains gives an additional diffraction peak (Figure 2). The calculation and experiment agree quite well and it can be concluded that the PEG- P(Asp(Bzl)) micelle is well described by the core−shell model. The inset of Figure 6 presents the electron density profile that gave the best fit. When we could not obtain good fitting after the polydispersity was included, we repeated the above procedure from the beginning until we obtained better results. One may consider that it would be better to iterate the fitting by simultaneously changing all parameters including the polydispersity. However, this method needs a good combination of initial parameters to converge the fitting.

Smearing of the scattering curve would be caused by the density gradient in the shell layer as well as the polydispersity in size. In this case, however, the density gradient in the shell layer causes only a small change in the scattering data because the electron density of the core is much higher than that of the shell (Supporting Information Figure S5). Therefore, we consider the polydispersity to be the major factor in smear the scattering curve.

Changes in Model Parameters upon Loading LE540. The above analysis gave ρ_S = 340 e/nm^3 for the LE540-unloaded micelle. Because LE540 is presumed to be incorporated only into the core, ρ_S should keep the same value during the loading of LE540. For the LE540-loaded micelles, we fitted the profiles under the condition that ρ_S = 340 e/nm^3, and ρ_C was treated as an adjustable parameter. The resultant curves are compared with the experiments in Figure 7 for L_{LE540} = 1.4 and 8.3 wt %, and the obtained parameters are summarized in Table 2. As presented in Figure 7, the agreement is very good. Figure 8 shows the relation between R_C and L_{LE540}. Here, we take $R_C{}^3$ to be the ordinate axis against L_{LE540} because the volumetric increment is expected to be proportional to the added amount. With increasing L_{LE540}, $R_C{}^3$ increases in a sigmoidal manner.

Aggregation Number and PEG Volume Fraction. Because the core consists of P(Asp(Bzl)), we can presume that its density is the same as that of the bulk state. On the basis of this assumption, the number of aggregated blocks in one micelle (N_{agg}) can be calculated with the following equation[37] by the use of V_C and a specific volume of P(Asp(Bzl)) ($\nu_{P(Asp(Bzl))}$ = 0.77 cm^3/g) determined for the amorphous state

$$N_{agg} = \frac{x_{P(Asp(Bzl))} V_C N_A}{M_{P(Asp(Bzl))} \nu_{P(Asp(Bzl))}} \quad (8)$$

where $x_{P(Asp(Bzl))}$ is the volume fraction of P(Asp(Bzl)) in the core. This is equal to 1 for the drug-unloaded core, and for LE540-loaded micelles, it was determined by the use of the density of LE540 (ca, 1.20 g cm^{-3}). $M_{(P(Asp(Bzl))}$ is the molecular weight of the P(Asp(Bzl)) block (= 4.6 × 10^3 g mol^{-1}) used in this work. The resultant N_{agg} values are listed in Table 2 and are seem to increase by about 35% upon addition of LE540. In this calculation, we assumed the same value of $\nu_{P(Asp(Bzl))}$. As presented in Figure 2, the addition of LE540 induced the disordering of the core. This means that $\nu_{P(Asp(Bzl))}$ should increase to some extent with an increase in L_{LE540}. Therefore, it might be possible that the actual increment in N_{agg} is smaller than in the present calculation.

(35) Sakajiri, K.; Kawasaki, E.-i.; Watanabe, J. *Macromolecules* **2001**, *34*, 7238–7240.

(36) Inomata, K.; Liu, L.-Z.; Nose, T.; Chu, B. *Macromolecules* **1999**, *32*, 1554–1558.

(37) Nakano, M.; Matsuoka, H.; Yamaoka, H.; Poppe, A.; Richter, D. *Macromolecules* **1999**, *32*, 697–703.

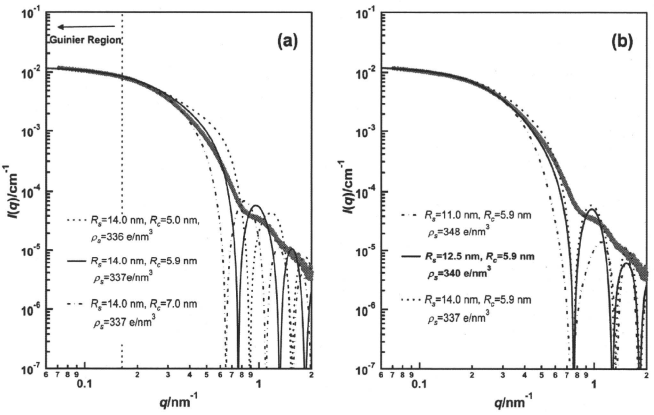

Figure 5. Comparison of the SAXS data and the theoretical values calculated from the core−shell model with R_g = 6.4 nm at L_{LE540} = 0. The same (a) R_S = 14.0 nm and the same (b) R_C = 5.9 nm are used.

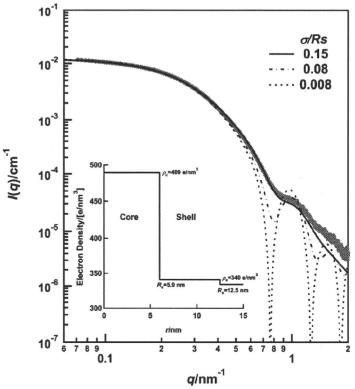

Figure 6. Smearing effect from the distribution and comparison with the data and calculations. The inset shows the electron density profile for the best-fit model.

Using the obtained N_{agg}, we can calculate the volume fraction of the PEG chain in the shell (f_{PEG}) by the following equation[37]

$$f_{PEG} = N_{agg}\frac{M_{PEG}\nu_{PEG}/N_A}{V_M - V_C} \quad (9)$$

where ν_{PEG} is the specific volume of PEG (= 0.893 cm^3 g^{-1}) and M_{PEG} is the molecular weight of the PEG chain (= 5.2 × 10^3 g mol^{-1}). The resultant f_{PEG} is listed in Table 2, showing that f_{PEG} is almost independent of L_{LE540} or slightly increased. The resultant f_{PEG} values lead to ρ_S = 339−341 e/nm^3 by the use of the relation $\rho_S = f_{PEG}\rho_{PEG} + (1 - f_{PEG})\rho_0$. By considering experimental errors in determining R_S as well as $M_{P(Asp(Bzl))}$ and M_{PEG}, we can consider that these values for ρ_S are consistent with those in Table 2. In particular, the very low contrast between the shell and the solvent limits the accuracy in the determined R_S. It should be noted that Nakano et al. obtained a similar value for the volume fraction of the shell chains although the chemical structure is different from that of PEG.[37]

The formation of the core−shell polymeric micelles from asymmetric block copolmers can be understood in the framework of packing parameter theory introduced by Israelachvili.[38] This theory rationalizes the shape of the micelle in terms of the volumetric balance between the head (i.e., hydrophilic) and tail (hydrophobic) groups. For polymeric micelles and for this volumetric balance, the elastic deformation of the core chains, the osmotic energy of the shell chains, and the interfacial tension between the core chains and the solvent have to be considered.[39,40] The relative significance of these three components is dependent on the number of chemical repeat units of the core (N_C) and the shell (N_S). In the present case, because of N_S (= 117) > N_C (= 24), the osmotic free energy should dominate. This is the reason that we assumed a constant ρ_S in the analysis.

Using the same technique as Riley et al.,[21] we determined the surface area available per PEG block at the core/shell interface (S_C/N_{agg}) and at the surface of the shell (S_S/N_{agg}), and the results are summarized in Table 2. Although S_C/N_{agg} slightly increased upon addition of LE540, it stayed in the range of 3.0−3.2 nm^{-2}. These values are much smaller than the cross-sectional area, πR_g^2 (~30 nm^2), of isolated PEG in water with M_{PEG} = 5.0 × 10^3 g mol^{-1} and R_g = 3.1 nm.[21] This suggests that the PEG chains in the PEG-P(Asp(Bzl) micelles are likely to interact with each other and take a brushlike configuration, as pointed out by Riley et al. Unchanged S_C/N_{agg} can be related to the aggregation number, and the micellar structure is mainly determined by the osmotic free energy of the PEG domain.

Structural Changes upon Adding LE540. As shown in Figure 2, this characteristic peak due to the periodic arrangement

(38) Israelachvili, J. N.; Mitchell, D. J.; Ninham, B. W. *J. Chem. Soc., Faraday Trans. 2* **1976**, *72*, 1525–1568.
(39) Izzo, D.; Marques, C. M. *Macromolecules* **1993**, *26*, 7189–7194.
(40) Halperin, A. *Macromolecules* **1987**, *20*, 2943–2946.

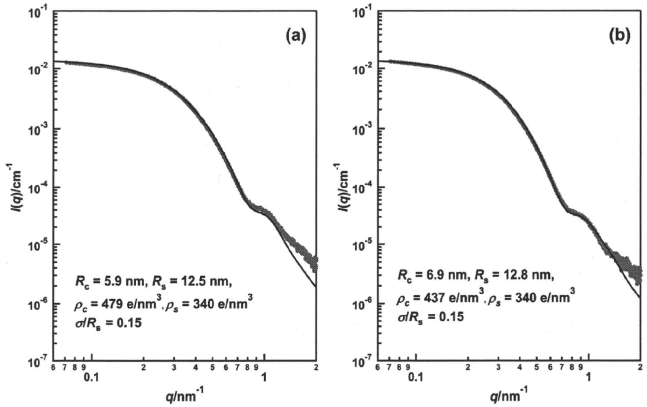

Figure 7. SAXS profiles of the micelle with L_{LE540} = 1.4 (a) and 8.3 wt % (b) and the best-fit calculations.

Table 2. Best Combination of the Fitting Parameters

L_{LE540} /wt % for PEG-P(Asp(Bzl))	R_C/nm	R_S/nm	ρ_C /e/nm^3	ρ_S /e/nm^3	σ/R_S	N_{agg}	f_{PEG}	S_C/N_{agg}/ nm^2	S_S/N_{agg}/ nm^2
0	5.9	12.5	489	340	0.15	145	0.15	3.0	14
1.4	5.9	12.5	479	340	0.15	142	0.15	3.1	14
3.0	6.1	12.3	454	340	0.15	148	0.16	3.2	13
5.8	6.7	12.5	444	340	0.15	177	0.19	3.2	11
8.3	6.9	12.8	437	340	0.15	182	0.19	3.2	11

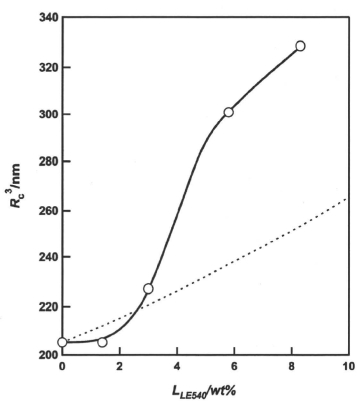

Figure 8. L_{LE540} dependence of R_C. The dashed line is calculated by assuming a simple expansion of the core by loading LE540.

of P(Asp(Bzl)) at q = 4 nm^{-1} almost disappeared at L_{LE540} > 4.0%. In accordance with this change, R_C showed a sigmoidal increase (Figure 8). If N_{agg} does not change and the added LE540 simply increases the core volume, then the relation of $R_C^3 \propto L_{LE540}$ should hold as presented as the dashed line in Figure 8. For this case, S_C/N_{agg} increases with L_{LE540} and reaches 3.6 nm^2 at L_{LE540} = 8.3 wt %. The increase in S_C/N_{agg} changes the PEG osmotic free energy in an unfavorable direction. To maintain the osmotic free energy at the minimum, N_{agg} is increased in addition of LE540. This is one reason for the large increase in R_C. Another reason is the attractive interaction and thus the solubility between LE540 and P(Asp(Bzl)). These two factors would generate the sigmoidal increase in R_C. The maximum in LE540 loading, L_{LE540}, can be determined by the upper limit of S_C/N_{agg} to maintain the minimum free energy including the elastic deformation of the core chains, the PEG osmotic energy, the interfacial tension, and the solubility between the core and LE540.

5. Conclusions

SAXS measurements were carried out on aqueous solutions of PEG-P(Asp(Bzl)) loaded with LE540 up to 8.3 wt %. Their scattering profiles could be characterized as an isolated spherical scattering object and confirmed the formation of core−shell micelles. Before the addition of LE540, a diffraction peak was observed around q = 4 nm^{-1} that was attributable to ordering between α-helices of P(Asp(Bzl)). This peak disappeared as LE540 was immersed in the core. This result can be interpreted by assuming that LE540 was uniformly distributed in the core. By use of a core−shell spherical micelle model, the SAXS data could be well fitted for all of the samples. R_C sigmoidally increased upon addition of LE540 from 5.9 to 6.9 nm, but R_S stayed between 12.5 and 12.8 nm and N_{agg} increased from 145 to 182. Finally, we believe that such good agreement between the theoretical calculation and the experimental SAXS result was possible only because of the SAXS experiments with an extremely high S/N ratio and extremely low parasitic scattering in the background.

Acknowledgment. This work was financially supported by the JST CREST program and the Ministry of Education and Science

via a grant-in-aid for I.A. (20550193). All SAXS measurements were carried out at SPring-8 40B2 (2008B0012 for K.S. and 1781 for I.A.).

Note Added after ASAP Publication. This article was published ASAP on April 2, 2010 with a misspelling in one author's name. The correct version was published on April 16, 2010.

Supporting Information Available: SAXS profiles from H_2O and from PEG-PBLA micelles. Guinier plots for PEG and ovalbumine. Relation of the adjustable parameters (R_C, R_S, and ρ_S) in numerical calculations with the core–shell sphere model for the PEG-PBLA micelle. Observation of the soft interface. This material is available free of charge via the Internet at http://pubs.acs.org.

Tohoku J. Exp. Med., 2010, **221**, 257-264

Convection-Enhanced Delivery of a Synthetic Retinoid Am80, Loaded into Polymeric Micelles, Prolongs the Survival of Rats Bearing Intracranial Glioblastoma Xenografts

Michiko Yokosawa,[1] Yukihiko Sonoda,[1] Shin-ichiro Sugiyama,[1] Ryuta Saito,[1] Yoji Yamashita,[1] Masamichi Nishihara,[2] Taku Satoh,[2] Toshihiro Kumabe,[1] Masayuki Yokoyama[2] and Teiji Tominaga[1]

[1]Department of Neurosurgery, Tohoku University Graduate School of Medicine, Sendai, Japan
[2]Yokoyama Nano-medical Polymers Project, Kanagawa Academy of Science and Technology, Kawasaki, Japan

Prognosis for the patients with glioblastoma, the most common malignant brain tumor, remains dismal. A major barrier to progress in treatment of glioblastoma is the relative inaccessibility of tumors to chemotherapeutic agents. Convection-enhanced delivery (CED) is a direct intracranial drug infusion technique to deliver chemotherapeutic agents to the central nervous system, circumventing the blood-brain barrier and reducing systemic side effects. CED can provide wider distribution of infused agents compared to simple diffusion. We have reported that CED of a polymeric micelle carrier system could yield a clinically relevant distribution of encapsulated agents in the rat brain. Our aim was to evaluate the efficacy of CED of polymeric micellar Am80, a synthetic agonist with high affinity to nuclear retinoic acid receptor, in a rat model of glioblastoma xenografts. We also used systemic administration of temozolomide, a DNA-alkylating agent, which has been established as the standard of care for newly diagnosed malignant glioma. U87MG human glioma cells were injected into the cerebral hemisphere of nude rats. Rats bearing U87MG xenografts were treated with CED of micellar Am80 (2.4 mg/m^2) on day 7 after tumor implantation. Temozolomide (200 mg/m^2/day) was intraperitoneally administered daily for 5 days, starting on day 7 after tumor implantation. CED of micellar Am80 provided significantly longer survival than the control. The combination of CED of micellar Am80 and systemic administration of temozolomide provided significantly longer survival than single treatment. In conclusion, temozolomide combined with CED of micellar Am80 may be a promising method for the treatment of malignant gliomas.

Keywords: Am80; glioblastoma; convection-enhanced delivery; temozolomide; polymeric micelle
Tohoku J. Exp. Med., 2010, **221** (4), 257-264.

Glioblastoma is the most common primary malignant brain tumor in adults. Despite therapeutic advances, the median survival continues to be approximately 12 months. Therefore, a new therapeutic approach is required.

Convection-enhanced delivery (CED) is a relatively new method that might overcome the problems posed by the requirements of local drug delivery (Bobo et al. 1994). CED uses a pressure gradient established at the tip of an infusion catheter to create bulk-flow that pushes the drug through the interstitial spaces. CED of therapeutic agents bypasses the blood-brain barrier, delivers high concentrations of therapeutic agents to the target site, and minimizes systemic exposure, thus resulting in fewer side effects. CED has been used to deliver many antineoplastic agents in animal studies with promising outcomes (Bruce et al. 2000; Degen et al. 2003; Vogelbaum 2007). However, CED of free drugs has various problems including rapid clearance from the tumor interstitium, so no selective accumulation in the targeted tissue can be achieved (Kunwar et al. 2007). We considered that it was necessary to develop a new pharmaceutical composition comprising an effective CED agent.

Drug carrier systems offer the advantage of sustained drug release as well as targeting of specific sites. Liposomes have been used as drug carriers in combination with CED (Saito et al. 2004, 2006a, 2006b; Noble et al. 2006; Yamashita et al. 2007; Kikuchi et al. 2008). Recently, we demonstrated the therapeutic efficacy of a newer type of drug carrier system, polymeric micellar doxorubicin, which was infused by CED in rat brain tumor models (Inoue et al. 2009). Polymeric micelles are an assembly of synthetic polymers, which typically block copolymers with both hydrophobic and hydrophilic properties. Polymeric micelle

Received March 10, 2010; revision accepted for publication June 17, 2010. doi:10.1620/tjem.221.257
Correspondence: Yukihiko Sonoda, M.D. Ph.D., Department of Neurosurgery, Tohoku University Graduate School of Medicine, 1-1, Seiryo-machi, Aoba-ku, Sendai, 980-8574, Japan.
e-mail: sono@nsg.med.tohoku.ac.jp

carrier systems were first studied for targeting solid tumors by intravenous injection (Yokoyama et al. 1990, 1999). Polymeric micelle carrier systems are electrically neutral and have the so-called stealth property that evades rapid clearance by the reticuloendothelial system. Consequently, systemic administration of polymeric micelle systems is effective against solid tumors because of the enhanced permeability and retention effect, which depends on the hyperpermeable vasculature and the absence of effective lymphatic drainage that prevents efficient clearance of macromolecules in the solid tumor tissues (Greish 2007). Various micelle-encapsulated cytotoxic agents are currently undergoing clinical evaluation for systemic administration, including doxorubicin (Tsukioka et al. 2002), paclitaxel (Hamaguchi et al. 2007), cisplatin (Uchino et al. 2005), and a camptothecin derivative SN-38 (Koizumi et al. 2006).

All-trans retinoic acid (ATRA) and other retinoids are reported to inhibit the growth rate of various malignancies including acute polymyelocytic leukemia, lung cancer, and glioblastoma both in vivo and in vitro (Flynn et al. 1983; Yung et al. 1996; Jaeckle et al. 2003). ATRA induces cell differentiation, cell cycle arrest, apoptotic cell death, and interleukin 6/interleukin 6 receptor downregulation in vitro. Retinoid effects are mediated through the interaction with two types of nuclear receptors, retinoic acid receptor (RAR) and retinoid X receptor (RXR), each of which has three subtypes (-α, -β, and -γ). ATRA is one of the most clinically effective retinoids; nevertheless, high rates of adverse effects have been reported such as exanthesis, fever, and xeroderma (Delva et al. 1993). The adverse effect on the skin is due to the large number of RAR-γ receptors distributed in the skin. The definition of retinoids has been expanded to include molecules that bind to RARs and RXRs, regardless of the similarity in molecular structure to ATRA. Am80 is such a synthetic retinoid with strong binding affinity to the nuclear receptors, but has a very different chemical structure to ATRA (Tobita et al. 1997). Am80 is a RAR-α/β-selective retinoid that does not activate RAR-γ and RXRs, so it may not cause adverse effects. Am80 is a promising candidate for CED infusion because glioma cells have extensive expression of RAR-α/β (Chattopadhyay et al. 2001; Costa et al. 2001). Alkylating agents and retinoids are among the chemotherapeutic agents that have shown activity against gliomas, either individually or in combination. Temozolomide and 13-cis-retinoic acid have also shown activity against recurrent gliomas in phase II clinical trials (Yung et al. 1996; Wismeth et al. 2004).

In the present study, we evaluated the efficacy of CED administration of micellar Am80 and/or systemic administration of temozolomide in the intracranial xenograft model.

Methods

Preparation of Agents

Am80 was kindly provided by Dr. Koichi Shudo of the Research Foundation Itsuu Laboratory (Tokyo, Japan). Temozolomide was provided by Schering-Plough K.K. (Osaka, Japan) and was dissolved in a solution of 0.1% dimethyl sulfoxide (Sigma Chemical Co., St. Louis, MO) in 0.9% NaCl solution.

Am80 was incorporated into a polymeric micelle formed from poly(ethylene glycol)-β-poly(benzyl aspartate) block copolymer. The polymer synthesis, Am80 incorporation into the polymeric micelle carrier, and characterization of the carrier system were as previously described (Satoh et al. 2009). Briefly, the block copolymer and Am80 were dissolved in tetrahydrofuran, and the obtained solution was subjected to solvent evaporation. Water was added to the dried residue, followed by sonication. The micelle solution was centrifuged to remove any insoluble precipitate (3,900 rpm, 10 min, 20°C) and then filtered through a Millex 0.22 μm PVDF filter (Millipore Corp, Billerica, MA). The composition of the block copolymer was as follows. The mean molecular weight of the poly(ethylene glycol) chain was 5,200, and the mean unit number of the poly(aspartic acid) chain was 24. Hydrophobic benzyl ester was formed at 83 mol% of the aspartic acid residue. Therefore, the mean molecular weight of the poly(aspartate) chain (83% benzyl aspartate residues and 17% aspartic acid residues) was 4600. In addition, N,N-dimethyloctadecylamine was added as a hydrophobic amine with Am80 at a molar ratio of 1:1 in the micelle preparation step. The drug content by weight in the polymeric micelle was 14%.

Tumor Cell Line

The established human glioblastoma cell line U87MG was obtained from the American Type Culture Collection (Rockville, MD). Cells were maintained as monolayers in a complete medium consisting of Eagle's minimal essential medium supplemented with 10% fetal calf serum, non-essential amino acids, and 100 U/ml penicillin G. Cells were cultured at 37°C in a humidified atmosphere consisting of 95% air and 5% CO_2.

Cell Viability Assay

The cell viability of U87MG cell lines treated with Am80 and temozolomide was assessed using the MTS assay (CellTiter96 Aqueous One Solution Cell Proliferation Assay; Promega Corp, Madison, WI). MTS, (3-(4,5-dimethylthiazol-2-yl)-5-(3-carboxymethoxyphenyl)-2-(4-sulfophenyl)-2H-tetrazolium), was reduced by living cells in the presence of phenazine methosulfate (PMS) to yield a purple formazan product that could be assayed colorimetrically. Cells were seeded at 750 cells per well in 75 μl of medium in 96-well flat-bottom plates and grown overnight at 37°C in an incubator. Temozolomide was used at 100 μM as described previously (Das et al. 2005). After exposure to Am80 (0, 50, 100, 200, or 500 μM), temozolomide (100 μM), and a combination of the two agents (100 μM Am80 + 100 μM temozolomide) for 24 hours, the plates were assayed with a microplate reader (Softmax Pro; Molecular Devices Corp, Sunnyvale, CA). Results were compared using one-way analysis of variance (ANOVA) with Tukey's Multiple Comparison test at a 95% confidence interval.

Western Blot Analysis

On the day before treatment, 1×10^6 cells per dish were seeded. After 24 hours incubation, cells were treated with Am80 (100 μM), temozolomide (100 μM), or a combination of both agents. Cells were collected 24 hours and 48 hours after the treatment. Protein was extracted from these cells with a mammalian protein extraction reagent (M-PER; Thermo Scientific, Rochester, NY). Samples were then prepared in sample buffer (Novex; Invitrogen, Carlsbad, CA) and

heated to 94°C for 5 minutes. Samples were then subjected to electrophoresis on 10% polyacrylamide gels (or 16% gels only for cleaved caspase-3), and then blotted onto polyvinylidene fluoride membranes (PDVF) (Invitrogen). PDVF were then incubated overnight with primary antibody against phospho-mitogen-activated protein kinase (phospho-MAPK) (Cell Signaling Technology, Cambridge, MA; 1:200), phospho-Akt (Cell Signaling Technology; 1:200), cleaved caspase-3 (Cell Signaling Technology; 1:500), cleaved caspase-9 (Cell Signaling Technology; 1:500), and β-actin (Santa Cruz Technology, Santa Cruz, CA; 1:1000). The residue targets for each phospho-specific antibody were p-MAPK (Thr202/Tyr204) and p-Akt (Thr308). The membranes were washed 3 times in Tris-buffered saline containing Tween 20, then incubated with secondary antibody for 60 minutes and subsequently washed. The blot was visualized with the ECL Plus Western Blotting Detection System (GE Healthcare Bioscience, Little Chalfont, Buckinghamshire, UK).

Animals

Male Sprague–Dawley rats weighing approximately 200 g were obtained from Charles-River Japan, Inc. (Yokohama, Kanagawa, Japan). Seven-week-old male Fischer 344/NJc1-rnu/rnu (nude) rats were purchased from CLEA Japan, Inc. (Tokyo, Japan). All protocols used in the animal studies were approved by the Institute for Animal Experimentation of Tohoku University Graduate School of Medicine.

Intracranial Tumor Implantation

U87MG cells were harvested by trypsinization, washed once with Hanks balanced salt solution without Ca^{2+} and Mg^{2+} (HBSS), and resuspended in HBSS for implantation. A cell suspension containing 5×10^5 cells per 10 μl of HBSS was used for implantation into the striatum of rat brains. Rats were placed in a small animal stereotactic frame (Narishige Manufacturing Co., Ltd., Japan) under deep halothane anesthesia. A sagittal incision was made through the skin to expose the cranium, and a burr hole was made in the skull at 0.5 mm anterior and 3 mm lateral from the bregma using a small dental drill. Cell suspension (5 μl) was injected at a depth of 4.5 mm from the brain surface. After a wait of 2 minutes, another 5 μl was injected at a depth of 4 mm. After a final wait of 2 minutes, the needle was removed, and the wound was closed with sutures.

CED

CED of micellar Am80, free Am80, or PBS was performed with a volume of 20 μl as described previously (Saito et al. 2006b). The infusion system consisted of a reflux free step-design infusion cannula connected to a loading line (containing micellar Am80, free Am80, or PBS) and an olive oil infusion line. A 1-ml syringe (filled with olive oil) mounted onto a micro-infusion pump (BeeHive; Bioanalytical Systems, West Lafayette, IN) regulated the flow of fluid through the system. On the basis of the chosen coordinates, the infusion cannula was mounted onto stereotactic holders and guided to the target region of the brain through the same burr holes made in the skull at tumor implantation. The following ascending infusion rates were applied for the 20-μl infusion: 0.2 μl/min for 15 minutes, 0.5 μl/min for 10 minutes, and 0.8 μl/min for 15 minutes.

Evaluation of Micellar Am80 Toxicity

Sprague–Dawley rats (3 rats in each group) received a single 20 μl CED infusion of micellar Am80. To ensure the safety of micellar Am80, the starting dose of 2.4 mg/m^2, available highest dose of micellar Am80, was chosen. The dose of 1.2 mg/m^2 and 0.6 mg/m^2 were also evaluated. Rats were monitored daily for survival, weekly for weight, and for general health (alertness, grooming, feeding, excreta, skin, fur, mucous membrane conditions, ambulation, breathing, and posture). The rats were euthanized 6 weeks after the CED treatment, and their brains were removed, fixed, sectioned (5 μm), and stained with hematoxylin and eosin and examined using a stereoscopic microscope (SZX7; Olympus Corp, Tokyo, Japan) and a light microscope (ECLIPSE 80i; Nikon Corp, Tokyo, Japan).

Survival Studies

Thirty rats implanted with U87MG tumor cells were randomly assigned to 6 groups of 5 rats: 1) a control group treated with CED of PBS (20 μl solution), 2) a group that underwent systemic treatment with temozolomide (200 mg/m^2/day), 3) a group treated with CED of free Am80 (2.4 mg/m^2 Am80 in a 20 μl solution), 4) a group treated with CED of micellar Am80 (2.4 mg/m^2 Am80 in a 20 μl solution), 5) a group that underwent systemic treatment with micellar Am80 (2.4 mg/m^2 Am80 in a 20 μl solution) and systemic treatment with temozolomide (200 mg/m^2/day), and 6) a group treated with CED of Am80 (2.4 mg/m^2 Am80 in a 20 μl solution) and systemic treatment with temozolomide (200 mg/m^2/day). CED infusion of free Am80 or micellar Am80 was performed on day 7 after tumor implantation. Systemic treatment with temozolomide consisted of a dose of 200 mg/m^2/day in a solution of 10% dimethyl sulfoxide in 0.9% NaCl solution for a total volume of 90 ml/m^2, which was intraperitoneally administered daily for 5 days, starting on day 7 after tumor implantation. Systemic treatment of micellar Am80 was performed by injection through the tail vein 7 days after tumor implantation. Rats were monitored daily for survival and general health. Survival rates in the treatment groups were compared using a log-rank test. Estimated survival was expressed as a Kaplan-Meier curve.

Terminal Deoxynucleotidyl Transferase dUTP Nick End Labeling (TUNEL) Staining

Eight rats implanted with U87MG tumor cells were randomly assigned to 4 groups of 2 rats: 1) a control group, 2) a group treated with CED of micellar Am80, 3) a group treated with systemic temozolomide, and 4) a group treated with CED of micellar Am80 and systemic temozolomide. Paraffin sections made from the brains of 2 rats from each group euthanized 12 days after tumor implantation were examined for apoptosis. The sections were deparaffinized followed by incubation with NaN_3 and H_2O_2 in PBS with 0.3% Triton-X for 20 minutes at room temperature. Then, the slides were washed 3 times with PBS. After incubation with terminal deoxynucleotidyl transferase (TdT) buffer (TdT, Recombinant; Invitrogen) for 15 minutes at room temperature, a mixture of TdT (2.5 μl) (Invitrogen), biotinylated 16-dUTP (6 μl) (Roche Diagnostics, Mannheim, Germany), and TdT buffer (100 μl) was added to each slide for 60 minutes at 37°C. Then, the slides were washed 2 times with TB buffer (6 mM sodium citrate, 60 mM NaCl) and blocked by incubation in 2% bovine serum albumin in PBS for 15 minutes at room temperature, followed by washing 3 times after blocking and incubation in an avidin-biotin peroxidase complex (ABC) solution (VECTASTAIN Elite ABC Standard Kit; Vector Laboratories Inc., Burlingame, CA) in PBS for 30 minutes at room temperature. The slides were twice washed with 0.175 M sodium acetate for 10 minutes and then reacted with 3′ 3-diaminobenzidine hydrochloride for appropriate times. Counterstaining was performed with methyl green solution.

Results

Enhanced Cytotoxic Effects of Am80 and Temozolomide In Vitro

Am80 significantly reduced the viability of U87MG cells in a dose-dependent manner through U87MG cells seeded in a 96-well flat-bottom plate and treated after 24 hours, then incubated for 2, 4, and 6 days (Fig. 1A). Inhibition of cell growth was high at 4 and 6 days after treatment. The 50% inhibition concentration (IC50) of Am80 was 123 μM. In combination with temozolomide, Am80 was used at 100 μM, approximate IC50 concentrations. Am80 combined with temozolomide achieved additional reduction in cell viability (Fig. 1B). Expression levels of phospho-Akt, phospho-MAPK, cleaved caspase-3, cleaved caspase-9, and β-actin were evaluated by western blot analysis using antibodies that detect only the phosphorylated forms of these proteins (Fig. 2). Treatment with Am80 or temozolomide showed a modest decrease in the expression of phospho-Akt protein, but treatment with Am80 and temozolomide further decreased the expression. Expression of phospho-MAPK was strongly suppressed in cells treated with Am80 or temozolomide, and the suppression effect was sustained in cells treated with these in combination. Western blot analyses for cleaved caspase-3 and cleaved caspase-9 indicated the activation of caspase-3 and caspase-9, respectively, in U87MG cells treated with temozolomide, Am80, or the combination of temozolomide and Am80. Similar levels of activation of both caspases were observed in the U87MG cells treated with temozolomide alone and Am80 alone. The combination of Am80 and temozolomide enhanced activation of both caspases. The molecular events occurring during synergistic induction of cell death due to temozolomide and Am80 were characterized in U87MG cells.

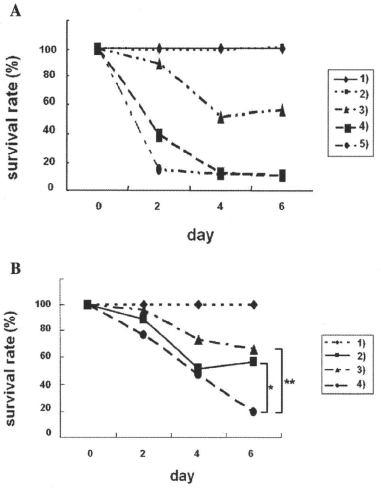

Fig. 1. Effects of Am80 and its combination with temozolomide on the viability of U87MG cells.
Shown are the effects of Am80 alone (A) and its combination with temozolomide (B) on the viability of U87MG cells, as determined by MTS assay. U87MG cells were seeded in a 96-well flat-bottom plate and incubated for 24 hours, then treated for 2, 4, and 6 days. Fig. 1A shows the dose-response effects of Am80: 1) 0 μM, 2) 50 μM, 3) 100 μM, 4) 200 μM, and 5) 500 μM. Fig. 1B shows the effects of 1) control, 2) 100 μM Am80, 3) 100 μM TMZ, and 4) 100 μM Am80 + 100 μM TMZ. Significant difference between Am80 treated cells and Am80 + TMZ treated cells was indicated with * ($p < 0.001$) and significant difference between TMZ treated cells and Am80 + TMZ treated cells was indicated by ** ($p < 0.001$).

Toxicity of Am80 in Normal Brain Parenchyma

No dose-limiting toxicity was found at 0.6, 1.2, or 2.4 mg/m^2. Animals that received CED of micellar Am80 at 2.4 mg/m^2 or less showed evidence of minor tissue damage at the site of the infusion cannula in the striatum, but no other apparent toxicity (Fig. 3).

Efficacy of Combined Micellar Am80 and Temozolomide in U87MG Brain Tumor Xenograft In Vivo

All rats from the control group had to be euthanized because of tumor progression between 12 to 16 days after implantation. Single treatment with CED of free Am80 showed no improvement in survival. In contrast, CED of micellar Am80 provided significantly longer survival (p = 0.019, log-rank test). Furthermore, the combination treatment of CED of micellar Am80 and systemic treatment of temozolomide provided significantly longer survival than the single treatment (p = 0.0027 compared with the CED of micellar Am80 group, p = 0.0018 compared with the temozolomide group). However, the combination of systemic administration of micellar Am80 and temozolomide did not achieve longer survival than systemic temozolomide alone (Fig. 4).

Detection of Apoptotic Cell Death after Treatment

TUNEL staining was performed on brain slices of rats from each group euthanized 6 days after treatment had started. Tumors from rats treated with CED of micellar Am80 and temozolomide exhibited decreased tumor density and increased number of TUNEL-positive cells compared with those from animals treated with only agent or control animals (Fig. 5).

Discussion

In the present study, we found that the CED of micellar Am80 provided long survival for rats bearing U87MG xenografts. We previously reported that micellar agents infused by CED were extensively distributed in normal rat

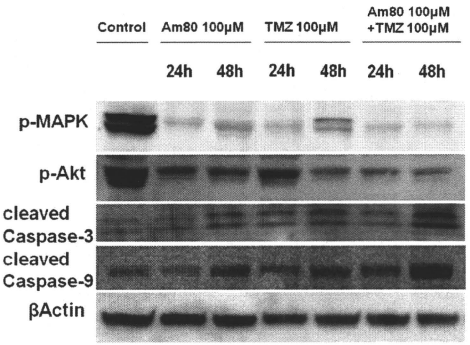

Fig. 2. Western blotting analysis for phospho-Akt, phospho-MAPK, cleaved caspase-3 and -9, and β-actin. The data shown are representative of three experiments.

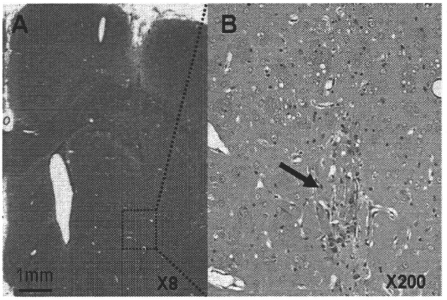

Fig. 3. Toxicity evaluation of micellar Am80 after CED infusion into the brain striatum of wild-type rats. There was only a slight cannulation scar; an arrow indicates small fibrous tissues with inflammation. No damage was induced to the infused hemisphere in any rats. Hematoxylin and eosin stain, original magnification × 8 in a stereoscopic microscope (A) and × 200 in a light microscope (B).

brain (Inoue et al. 2009). We also reported that micellar agents were distributed over almost the entire tumor area, including tumor margins, in rat brain tumor models (Inoue et al. 2009). The distribution of agents infused by CED in the rat brain is significantly increased if the infusate is more hydrophilic, which implies less tissue affinity (Saito et al. 2004, 2006b; MacKay et al. 2005; Yamashita et al. 2007). Furthermore, polyethylene glycol encapsulation provides steric stabilization, reduces surface charge, and achieves better distribution (Inoue et al. 2009). In the present study, the poorer brain/tumor tissue distribution caused by Am80 hydrophobicity might be overcome by polymeric micelle carrier system.

On the other hand, micellar Am80 administered intravenously did not contribute to long survival for rats bearing U87MG xenografts, despite the fact that micellar agents have been shown to accumulate around tumor vessels and effectively pass through brain tumor vessels (Kuroda et al. 2009). Although this study lacks monitoring or confirmation of infusate, it is speculated that micellar Am80 administered systemically could not sufficiently penetrate into the hypovascular central area of implanted tumor with three-dimensional cellular structures, in which the diffusion of infusate was restricted. Development of monitoring of the distribution of infusate is required to gain a deeper appreciation of micellar Am80.

Several chemotherapeutic agents delivered locally using CED, including 1,3-bis(chloroethyl)-1-nitrosourea (Bruce et al. 2000), gemcitabine, and carboplatin (Degen et al. 2003), prolonged survival of rats bearing U87MG xeno-

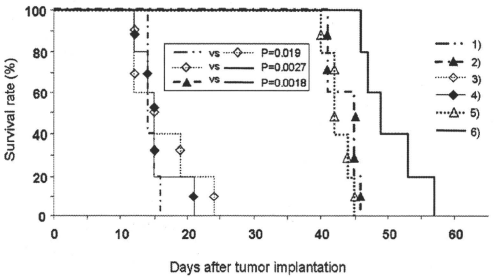

Fig. 4. Survival of treated animals bearing intracranial glioblastoma xenografts.
Survival of treated animals is expressed as a Kaplan-Meier curve (5 rats per each group). Rats bearing intracranial glioblastoma xenografts were treated with 1) vehicle (control), 2) systemic temozolomide (200 mg/m^2/day), 3) CED of the free Am80 (2.4 mg/m^2), 4) CED of micellar Am80 (2.4 mg/m^2), 5) combination of systemic treatment of micellar Am80 (2.4 mg/m^2) and temozolomide (200 mg/m^2/day), and 6) combination of CED of micellar Am80 (2.4 mg/m^2) and systemic temozolomide (200 mg/m^2/day). p-Values were obtained using a log-rank test.

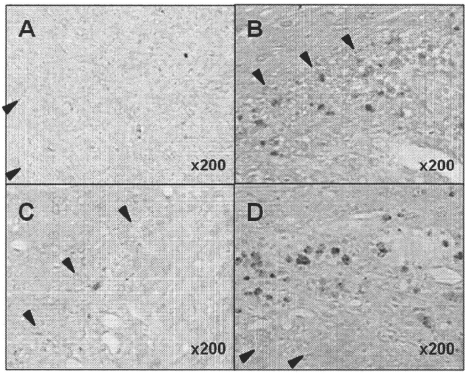

Fig. 5. Histological estimation with TUNEL staining. Brain slices of rats from each group were examined 12 days after tumor implantation. TUNEL-positive cells are stained brown. Arrowheads indicate the margin of xenografts. Counterstaining with methyl green, original magnification × 200. A: control group, B: group treated with CED of micellar Am80, C: group treated with systemic temozolomide, D: group treated with CED of micellar Am80 and systemic temozolomide.

grafts. However, some of these agents applied locally to the cerebrospinal fluid have long-term side effects including leukoencephalopathy and brain atrophy (Shapiro and Young 1984). Ideally, agents for CED administration into brain tumors would show the highest possible therapeutic ratio against tumor cells over normal cells. Retinoids such as Am80 show selective toxicity against neoplastic transformed cells, so they represent an excellent candidate for local delivery (Schneider et al. 2000). In our study, the toxicity of Am80 against normal brain cells was minimal, even with enhanced delivery. These results suggest that CED-delivered Am80 may be a viable therapeutic option (Chattopadhyay et al. 2001).

The most important function of the carrier is the inhibition of rapid drug absorption by cells at the injection site, since the agent cannot be distributed over a large volume of tissue in the presence of rapid absorption. Sustained drug release is needed for effective inhibition of rapid drug absorption by cells. In this study, we prepared polymeric micelles containing Am80, which were observed to sustain

the release of Am80 in vitro more than that of free Am80 (Satoh et al. 2009). For this reason, CED of this micelle was more effective than that of the free agent.

We chose temozolomide as a drug in combination with Am80 because the use of temozolomide is already clinically established for glioma therapy. The strategy for induction of differentiation followed by activation of apoptosis has been highly promising in cancer therapy. We found that Am80 and/or temozolomide treatment down-regulated cell growth signaling, p-MAPK. Activation of Akt is a major event in the development of glioblastoma, and high levels of Akt were frequently expressed in glioblastoma (Sonoda et al. 2001; Choe et al. 2003). Phosphorylation of Akt results in activation of Akt kinase activity, which has the potential to deregulate the cell cycle and suppress apoptosis. The present study demonstrated that treatment of U87MG xenografts with Am80 and temozolomide down-regulated phospho-Akt and activated cleaved caspase-3 and -9, indicating activation of the caspase cascade for apoptosis. In the survival study, CED of micellar Am80 individually or in combination with temozolomide improved the therapeutic outcome in the human glioblastoma model.

Agents such as temozolomide combined with CED administration of micellar Am80 may be promising for the treatment of malignant gliomas.

References

Bobo, R.H., Laske, D.W., Akbasak, A., Morrison, P.F., Dedrick, R.L. & Oldfield, E.H. (1994) Convection-enhanced delivery of macromolecules in the brain. *Proc. Natl. Acad. Sci. USA*, **91**, 2076-2080.

Bruce, J.N., Falavigna, A., Johnson, J.P., Hall, J.S., Birch, B.D., Yoon, J.T., Wu, E.X., Fine, R.L. & Parsa, A.T. (2000) Intracerebral clysis in a rat glioma model. *Neurosurgery*, **46**, 683-691.

Chattopadhyay, N., Butters, R.R. & Brown, E.M. (2001) Agonists of the retinoic acid- and retinoid X-receptors inhibit hepatocyte growth factor secretion and expression in U87 human astrocytoma cells. *Brain Res. Mol. Brain Res.*, **87**, 100-108.

Choe, G., Horvath, S., Cloughesy, T.F., Crosby, K., Seligson, D., Palotie, A., Inge, L., Smith, B.L., Sawyers, C.L. & Mischel, P.S. (2003) Analysis of the phosphatidylinositol 3′-kinase signaling pathway in glioblastoma patients in vivo. *Cancer Res.*, **63**, 2742-2746.

Costa, S.L., Paillaud, E., Fages, C., Rochette-Egly, C., Plassat, J.L., Jouault, H., Perzelova, A. & Tardy, M. (2001) Effects of a novel synthetic retinoid on malignant glioma in vitro: inhibition of cell proliferation, induction of apoptosis and differentiation. *Eur. J. Cancer*, **37**, 520-530.

Das, A., Banik, N.L., Patel, S.J. & Ray, S.K. (2004) Dexamethasone protected human glioblastoma U87MG cells from temozolomide induced apoptosis by maintaining Bax:Bcl-2 ratio and preventing proteolytic activities. *Mol. Cancer*, **3**, 36.

Degen, J.W., Walbridge, S., Vortmeyer, A.O., Oldfield, E.H. & Lonser, R.R. (2003) Safety and efficacy of convection-enhanced delivery of gemcitabine or carboplatin in a malignant glioma model in rats. *J. Neurosurg.*, **99**, 893-898.

Delva, L., Cornic, M., Balitrand, N., Guidez, F., Miclea, J.M., Delmer, A., Teillet, F., Fenaux, P., Castaigne, S., Degos, L. & Chomienne, C. (1993) Resistance to all-trans retinoic acid (ATRA) therapy in relapsing acute promyelocytic leukemia: study of in vitro ATRA sensitivity and cellular retinoic acid binding protein levels in leukemic cells. *Blood*, **82**, 2175-2181.

Flynn, P.J., Miller, W.J., Weisdorf, D.J., Arthur, D.C., Brunning, R. & Branda, R.F. (1983) Retinoic acid treatment of acute promyelocytic leukemia: in vitro and in vivo observations. *Blood*, **62**, 1211-1217.

Greish, K. (2007) Enhanced permeability and retention of macromolecular drugs in solid tumors: a royal gate for targeted anticancer nanomedicines. *J. Drug Target*, **15**, 457-464.

Hamaguchi, T., Kato, K., Yasui, H., Morizane, C., Ikeda, M., Ueno, H., Muro, K., Yamada, Y., Okusaka, T., Shirao, K., Shimada, Y., Nakahama, H. & Matsumura, Y. (2007) A phase I and pharmacokinetic study of NK105, a paclitaxel-incorporating micellar nanoparticle formulation. *Br. J. Cancer*, **97**, 170-176.

Inoue, T., Yamashita, Y., Nishihara, M., Sugiyama, S., Sonoda, Y., Kumabe, T., Yokoyama, M. & Tominaga, T. (2009) Therapeutic efficacy of a polymeric micellar doxorubicin infused by convection-enhanced delivery against intracranial 9L brain tumor models. *Neuro. Oncol.*, **11**, 151-157.

Jaeckle, K.A., Hess, K.R., Yung, W.K., Greenberg, H., Fine, H., Schiff, D., Pollack, I.F., Kuhn, J., Fink, K., Mehta, M., Cloughesy, T., Nicholas, M.K., Chang, S. & Prados, M. (2003) Phase II evaluation of temozolomide and 13-cis-retinoic acid for the treatment of recurrent and progressive malignant glioma: a North American Brain Tumor Consortium study. *J. Clin. Oncol.*, **21**, 2305-2311.

Kikuchi, T., Saito, R., Sugiyama, S., Yamashita, Y., Kumabe, T., Krauze, M., Bankiewicz, K. & Tominaga, T. (2008) Convection-enhanced delivery of polyethylene glycol-coated liposomal doxorubicin: characterization and efficacy in rat intracranial glioma models. *J. Neurosurg.*, **109**, 867-873.

Koizumi, F., Kitagawa, M., Negishi, T., Onda, T., Matsumoto, S., Hamaguchi, T. & Matsumura, Y. (2006) Novel SN-38-incorporating polymeric micelles, NK012, eradicate vascular endothelial growth factor-secreting bulky tumors. *Cancer Res.*, **66**, 10048-10056.

Kunwar, S., Prados, M.D., Chang, S.M., Berger, M.S., Lang, F.F., Piepmeier, J.M., Sampson, J.H., Ram, Z., Gutin, P.H., Gibbons, R.D., Aldape, K.D., Croteau, D.J., Sherman, J.W. & Puri, R.K. (2007) Direct intracerebral delivery of cintredekin besudotox (IL13-PE38QQR) in recurrent malignant glioma: a report by the Cintredekin Besudotox Intraparenchymal Study Group. *J. Clin. Oncol.*, **25**, 837-844.

Kuroda, J., Kuratsu, J., Yasunaga, M., Koga, Y., Saito, Y. & Matsumura, Y. (2009) Potent anticancer effect of SN-38-incorpotrating polymeric micelle, NK012, against malignant glioma. *Int. J. Cancer*, **124**, 2505-2511.

MacKay, J.A., Deen, D.F. & Szoka, F.C., Jr. (2005) Distribution in brain of liposomes after convection enhanced delivery; modulation by particle charge, particle diameter, and presence of steric coating. *Brain Res.*, **1035**, 139-153.

Noble, C.O., Krauze, M.T., Drummond, D.C., Yamashita, Y., Saito, R., Berger, M.S., Kirpotin, D.B., Bankiewicz, K.S. & Park, J.W. (2006) Novel nanoliposomal CPT-11 infused by convection-enhanced delivery in intracranial tumors: pharmacology and efficacy. *Cancer Res.*, **66**, 2801-2806.

Saito, R., Bringas, J.R., McKnight, T.R., Wendland, M.F., Mamot, C., Drummond, D.C., Kirpotin, D.B., Park, J.W., Berger, M.S. & Bankiewicz, K.S. (2004) Distribution of liposomes into brain and rat brain tumor models by convection-enhanced delivery monitored with magnetic resonance imaging. *Cancer Res.*, **64**, 2572-2579.

Saito, R., Krauze, M.T., Noble, C.O., Drummond, D.C., Kirpotin, D.B., Berger, M.S., Park, J.W. & Bankiewicz, K.S. (2006a) Convection-enhanced delivery of Ls-TPT enables an effective, continuous, low-dose chemotherapy against malignant glioma xenograft model. *Neuro. Oncol.*, **8**, 205-214.

Saito, R., Krauze, M.T., Noble, C.O., Tamas, M., Drummond, D.C., Kirpotin, D.B., Berger, M.S., Park, J.W. & Bankiewicz, K.S.

(2006b) Tissue affinity of the infusate affects the distribution volume during convection-enhanced delivery into rodent brains: implications for local drug delivery. *J. Neurosci. Methods*, **154**, 225-232.

Satoh, T., Higuchi, Y., Kawakami, S., Hashida, M., Kagechika, H., Shudo, K. & Yokoyama, M. (2009) Encapsulation of the synthetic retinoids Am80 and LE540 into polymeric micelles and the retinoids' release control. *J. Control Release*, **136**, 187-195.

Schneider, S.M., Offterdinger, M., Huber, H. & Grunt, T.W. (2000) Activation of retinoic acid receptor a is sufficient for ful induction of retinoid responses in SK-BR-3 and T47D Human brest cancer cells. *Cancer Res.*, **60**, 5479-5487.

Shapiro, W.R. & Young, D.F. (1984) Neurological complications of antineoplastic therapy. *Acta Neurol. Scand. Suppl.*, **100**, 125-132.

Sonoda, Y., Ozawa, T., Aldape, K.D., Deen, D.F., Berger, M.S. & Pieper, R.O. (2001) Akt pathway activation converts anaplastic astrocytoma to glioblastoma multiforme in a human astrocyte model of glioma. *Cancer Res.*, **61**, 6674-6678.

Tobita, T., Takeshita, A., Kitamura, K., Ohnishi, K., Yanagi, M., Hiraoka, A., Karasuno, T., Takeuchi, M., Miyawaki, S., Ueda, R., Naoe, T. & Ohno, R. (1997) Treatment with a new synthetic retinoid, Am80, of acute promyelocytic leukemia relapsed from complete remission induced by all-trans retinoic acid. *Blood*, **90**, 967-973.

Tsukioka, Y., Matsumura, Y., Hamaguchi, T., Koike, H., Moriyasu, F. & Kakizoe, T. (2002) Pharmaceutical and biomedical differences between micellar doxorubicin (NK911) and liposomal doxorubicin (Doxil). *Jpn. J. Cancer Res.*, **93**, 1145-1153.

Uchino, H., Matsumura, Y., Negishi, T., Koizumi, F., Hayashi, T., Honda, T., Nishiyama, N., Kataoka, K., Naito, S. & Kakizoe, T. (2005) Cisplatin-incorporating polymeric micelles (NC-6004) can reduce nephrotoxicity and neurotoxicity of cisplatin in rats. *Br. J. Cancer*, **93**, 678-687.

Vogelbaum, M.A. (2007) Convection enhanced delivery for treating brain tumors and selected neurological disorders: symposium review. *J. Neurooncol.*, **83**, 97-109.

Wismeth, C., Hau, P., Fabel, K., Baumgart, U., Hirschmann, B., Koch, H., Jauch, T., Grauer, O., Drechsel, L., Brawanski, A., Bogdahn, U. & Steinbrecher, A. (2004) Maintenance therapy with 13-cis retinoid acid in high-grade glioma at complete response after first-line multimodal therapy—a phase-II study. *J. Neurooncol.*, **68**, 79-86.

Yamashita, Y., Krauze, M.T., Kawaguchi, T., Noble, C.O., Drummond, D.C., Park, J.W. & Bankiewicz, K.S. (2007) Convection-enhanced delivery of a topoisomerase I inhibitor (nanoliposomal topotecan) and a topoisomerase II inhibitor (pegylated liposomal doxorubicin) in intracranial brain tumor xenografts. *Neuro. Oncol.*, **9**, 20-28.

Yokoyama, M., Miyauchi, M., Yamada, N., Okano, T., Sakurai, Y., Kataoka, K. & Inoue, S. (1990) Characterization and anticancer activity of the micelle-forming polymeric anticancer drug adriamycin-conjugated poly(ethylene glycol)-poly(aspartic acid) block copolymer. *Cancer Res.*, **50**, 1693-1700.

Yokoyama, M., Okano, T., Sakurai, Y., Fukushima, S., Okamoto, K. & Kataoka, K. (1999) Selective delivery of adriamycin to a solid tumor using a polymeric micelle carrier system. *J. Drug Target*, **7**, 171-186.

Yung, W.K., Kyritsis, A.P., Gleason, M.J. & Levin, V.A. (1996) Treatment of recurrent malignant gliomas with high-dose 13-cis-retinoic acid. *Clin. Cancer Res.*, **2**, 1931-1935.